UNIVERSITY OF TWENTE
FACULTY OF SCIENCE AND TECHNOLOGY
MESOSCALE CHEMICAL SYSTEMS GROUP
MASTER THESIS

Passive removal of electrochemically produced hydrogen gas in a microfluidic device

Author:
Samuel Mok, BSc.

Supervisors:
Professor Dr. Han Gardeniers
Assistant Professor Dr. David Fernandez Rivas
Dr. Fer Coenders

Abstract

The goal of this research is to create a microfluidic device where hydrogen is produced by electrolysis of water, while incorporating a method for the passive removal of the hydrogen gas from the microfluidic channels. To accomplish this, a number of microfluidic devices were designed, produced and tested. The main components of the final device are: a porous silicon membrane to be able to separately produce oxygen and hydrogen gas; platinum electrodes for the catalytic electrolysis of water; and channels with a tapered geometry to direct the gas bubbles in a certain direction without the need for an external pumping mechanism. After producing and testing the device it was shown the gas moves in the predicted direction, which proves the tapered channels work as expected. There is no definite proof that the two produced streams of gas are hydrogen and oxygen without cross-contamination, but no irregularities were observed to indicate otherwise. A similar current was needed for the electrolysis of water in the device with a membrane compared to a device with inter-digital electrodes, which indicates the membrane is not the limiting factor in electrolysis. For future research, the main recommendations are to keep incorporating the porous silicon membrane, platinum electrodes, and the tapered channels. Improvements can be made by reducing complexity and increasing usability, and incorporating measurement electrodes for accurate electrical measurements.

March 29, 2017
Enschede, The Netherlands

Contents

List of Figures

1. Introduction

This research is part of the Solar to Fuel Chip (S2FC) project, which is part of the larger BioSolar Cells research project. The aim of this research is to design and test a microfluidic device that can produce hydrogen by electrolyzing water, while incorporating a method for the passive removal of hydrogen gas form this device. Although it is already possible to electrolyze water in a microfluidic chip and produce energy with micro-solar cells, they are not yet available in an integrated form. By combining existing and new technology the S2FC project aims to create a single device that uses water and solar radiation to produce fuel.

To start this report, a short overview of current microfluidic technology is given, followed by a section on hydrogen production and current state of the art. This introductory chapter will be finished by stating the research motivation and goal.

1.1. Microfluidic technology

Microfluidics is the field that studies fluid mechanics in systems with characteristic dimensions at the micro-scale, such as nano-/micrometer diameters or pico-/nanoliter volumes. Devices of this size scale have interesting properties compared to larger ones, for instance a high surface area to volume ratio, the small amount of chemicals needed for analysis, and almost exclusively laminar flows for liquids at typical operating conditions (Re numbers between 1 and 100 are easily achieved). [1]

Another effect of the small size of the channels is that the balance of forces acting on fluids is different than in the macro-scale systems. In a microfluidic system inertial forces, which are normally predominant, are surpassed in strength by other forces like capillary action. A microfluidic chip (MFC) is a device that incorporates microfluidic channels. The channels in a MFC are usually made by chemical etching, the same process that is used to produce the microchips used in electronics.

The properties of MFCâĂŹs allow for unique applications, for example disposable units to check for certain diseases or a small chip to analyze DNA, miniature inkjet printers, thermal management chips, portable biological weapon detectors, and more. [2]

Microfluidic devices are used in this research because of portability, low cost and the ease of using capillary forces to process gas bubbles.

1.2. Hydrogen production

The goal of this research is to produce gaseous hydrogen. This element can be used either directly as a fuel, or it can be processed further into hydrocarbon fuels like methane. In Fig. 1.1 methods for the production of hydrogen are shown. Currently, 95% of hydrogen is obtained from fossil fuels like natural gas, oil or coal. Most of the rest is produced by electrolysis of water. However, the electricity that is used for that process is mostly produced by the same fossil fuels. As fossil fuels are slowly running out and produce large quantities of greenhouse gases, a different method for producing hydrogen is preferred.

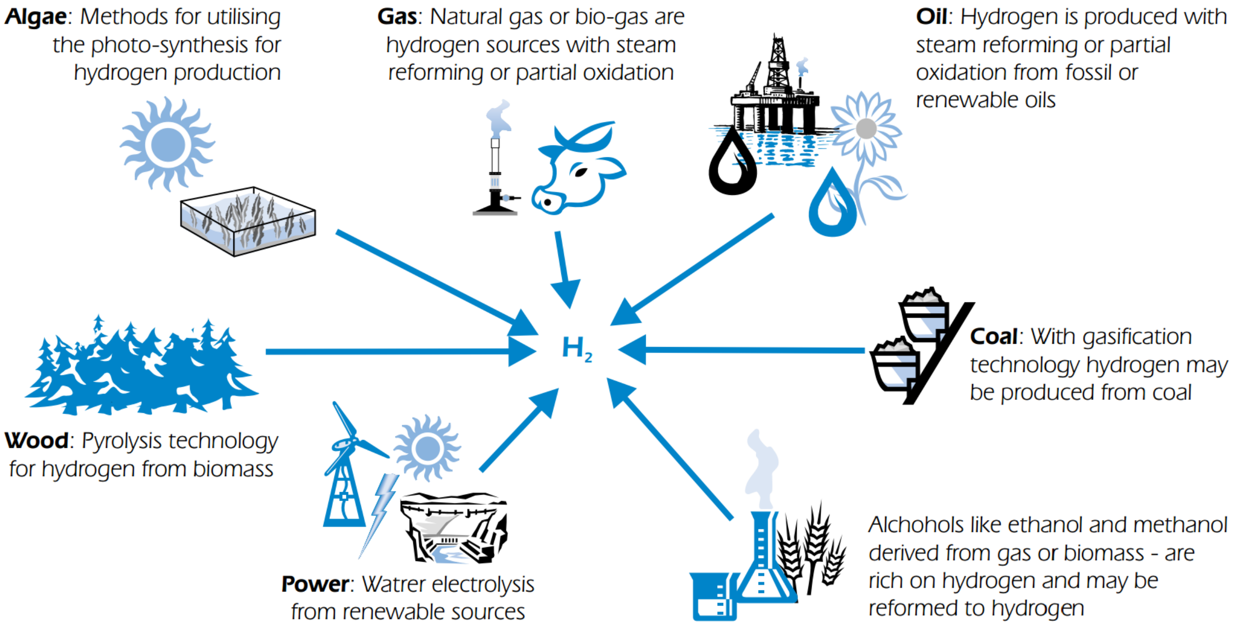

Figure 1.1: Various methods to produce hydrogen gas. [3]

The chosen method for this research is to use electrolysis of water. In this process electricity is used to split water into oxygen and hydrogen gas. For electrolysis several things are needed: a power source to supply the electrons, water with added ions for better conductivity, and a membrane to transport the protons from the anode to the cathode while keeping the resulting gases separated. If a membrane is not used, oxygen and hydrogen will mix, forming an explosive mixture that is very hard to separate again.

In this project, the eventual power source will be solar energy. By using a photo-voltaic device, photons can be used to produce electrons, which can then be used in the electrolysis. In the first stage of this research the photo-voltaic devices will not be used for the sake of simplicity. Instead, metal electrodes connected to a power supply will provide the necessary energy for electrolysis.

The use of a membrane is a key issue for this project. The reasons for this will be expanded upon later in this thesis. Membranes are often expensive and degrade on small timescales, especially compared to silicon devices. Multiple membranes will need to be tested and compared so the best option can be chosen.

Both electrolysis and membranes will be discussed more in-depth in Chapter 2: Electrolysis of Water and Chapter 4: Proton Transport .

1.3. Current state-of-the-art

Using solar energy to perform water splitting is currently a hot topic [4]. Multiple research groups around the world are currently exploring different avenues of approach to produce these so called solar fuels [5].

For solar fuel generators to be successful, economically viable designs need to be used, and the devices need to function under standard conditions for prolonged periods of time. At the moment, no single device has been made that satisfies these conditions [5]. There are multiple issues that still need to be solved in this regard, focusing on robustness under corroding environments and the efficient transport of ions inside a device [6].

Most research in this area focuses on individual parts of the problem, and even though a lot of progress has been made in that regard, the integration of the individual parts is a practical problem that also needs to be solved.

1.4. Goals of this research

As stated earlier in this report, the main goal is to produce hydrogen on a microfluidic chip by electrolysis. As this entails a combination of multiple parts, this main goal is split into multiple sub-goals.

The first sub-goal is to incorporate electrodes inside a microfluidic device. These electrodes will be used in conjunction with a power source for the electrolysis of water. In later stages of this research, the power source will be an on-chip photo-voltaic array, but initially it will be a conventional direct power supply.

The second sub-goal is to examine a method to passively (or in an energy-efficient way) transport the produced gas. The hydrogen that is produced will eventually be used as a fuel, so the less energy that is lost during production, the better. Moving parts are also to be avoided, as this will save on repair costs and downtime.

The third sub-goal is to produce oxygen and hydrogen in separate streams on the device. The most obvious manner to reach this goal is to incorporate a proton-conducting membrane in the system. The separate streams will save on costs, as the gas mixture does not need to be separated afterwards, and it also adds to the safety of operation as a mixture of hydrogen and oxygen is highly explosive.

These three goals lead to three separate topics: transport of gas bubbles, the electrolysis of water, and membranes to transport protons. These three topics are first treated separately in this thesis in Chapter 2: Electrolysis of Water, Chapter 3: Gas Transport, and Chapter 4: Proton Transport respectively. The results of the three sub-goals will be combined into a final design which will be discussed in chapter Chapter 5: Integrating & Combining. The report will end with recommendations for future research in this project.

2. Electrolysis of Water

Multiple methods can be used to produce hydrogen, as outlined in Section 1.2: Hydrogen production. The method chosen for this project is the electrolysis of water. This is the most straight forward method and it only requires water and electricity. In this chapter more theoretical background on electrolysis is given, followed by an explanation of the method used to perform electrolysis on a microfluidic device. This chapter finishes with the results of these preliminary tests. These results will be used in the final design as outlined in Chapter 5: Integrating & Combining.

2.1. Electrolysis: Theoretical Background

Electrolysis is the process where direct electrical current is used to break apart molecular bonds. [7] By adding electrons to a solution containing molecules that are able to undergo redox reactions, new compounds can be formed. Eq. 2.1 and eq. 2.2 show the two half reactions that take place during the electrolysis of water, followed by the overall reaction in eq. 2.3. Note that this set of reactions is balanced using acid (H^+) [7].

$$2\,H_2O \longrightarrow O_2 + 4\,H^+ + 4\,e^- \tag{2.1}$$

$$4\,H^+ + 4\,e^- \longrightarrow 2\,H_2 \tag{2.2}$$

$$2\,H_2O \longrightarrow O_2 + 2\,H_2 \tag{2.3}$$

In order to apply the current, a direct current power supply is connected to a cathode and an anode. The reduction of the hydrogen ions will take place at the cathode, and the oxidation of water will take place at the anode. The electrons will travel through the solution from the cathode to the anode. This process is also show in Fig. 4.1. The potential that is needed for this reaction is 1.24V vs RHE [8]. However, because of experimental losses an overpotential is almost always needed to start the electrolysis reaction [9]. This overpotential depends on the system used: the anode, cathode, membrane and used fluid. The usage of an electrode that also functions as an electrocatalyst is therefore highly preferred. For a water splitting reaction platinum is mostly used, as it is the most effective catalyst [9], while also being highly resistant to corrosion. One downside of platinum is that it is not transparent. As this device will eventually need solar power to function, light needs to penetrate into the chip. A transparent electrode is therefore preferred. Besides being opaque, platinum is also expensive (around 32 euro per gram [10]), so a more economic option should be investigated. In the final design of the chip, the electrodes will not be supplied by a DC power supply, but by a photovoltaic device. It is also possible to replace the electrodes with an photoelectrode, which directly uses solar energy to split the water [4]. This step is beyond the scope of this thesis, but is a clear goal of the overall research concerning solar-to-fuel cells.

2.2. Electrolysis: Materials and Methods

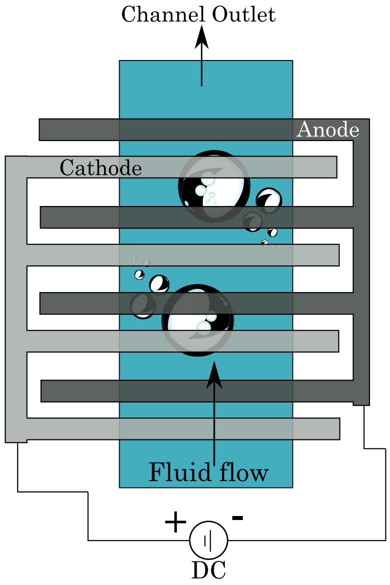

Figure 2.1: Electrolysis of water using a interdigital electrodes and a fluidic channel. This will create a mixture of hydrogen and oxygen in the channel if enough voltage is applied.

Two different electrode types will be investigated. As mentioned in Section 2.1: Electrolysis: Theoretical Background, platinum should perform the best, but is expensive and opaque. A cheaper and transparent material is also needed. To fulfull this role, indium tin oxide will be used. This is one of the most widely used transparent conducting materials [11].

To be able to test these electrodes in a proper environment, they are implemented as part of a microchip consisting of a silicon substrate and a glass cap. The chip will feature a microfluidic channel to supply the liquid to be electrolyzed. The electrodes will be added in an interdigital formation, which makes sure the distance between each anode and cathode pair is minimized [12]. A sketch of the principle of design is shown in Fig. 2.1.

Because this research consists of multiple parts, not only the electrodes are tested in this testing device. Multiple parts that need experimental testing are integrated into each produced microchip. This means the used chip also contains elements that are not explained in this chapter. An overview of components in the used chip is shown in Fig 2.2.

The electrodes will be sputtered on a glass substrate (MEMPax, 100 mm diameter, 500 µm thickness, Schott), which in turn is anodically bonded to a silicon substrate (100 mm diameter, 525 µm thick, Okmetic, Finland) that contains the etched channels (300 µm to 600 µm wide and 50 µm deep) that transport the liquid. To ensure electric isolation between the electrodes and the silicon, a 525 µm thick nitride enriched silicon layer is deposited on the silicon substrate using low pressure chemical vapor deposition. Once the substrates are bonded, deep reactive ion etching (DRIE) is used to create access holes 1 mm in diameter for fluid and electric connections.

The electrical connections are made using copper wires glued to the electrode layer using conducting silver epoxy. These wires are in turn connected to a DC power supply using crocodile clips. The electrolyte used in these test is a 1 mol/l sodium sulfate solution. This fluid is pumped by means of a syringe pump

(Harvard PHD2000) combined with 3 mL plastic syringes (BD Integra w/ Luer-Lok fitting) connected to the chip using capillary tubing (Polymicro, outer diameter 360 µm) and various fittings/connectors by Upchurch. Optical measurements are made using an inverted microscope (Leica, DMI5000M) combined with a digital camera (Leica, DFC300FX). A sketch of the setup is shown in Fig 2.3.

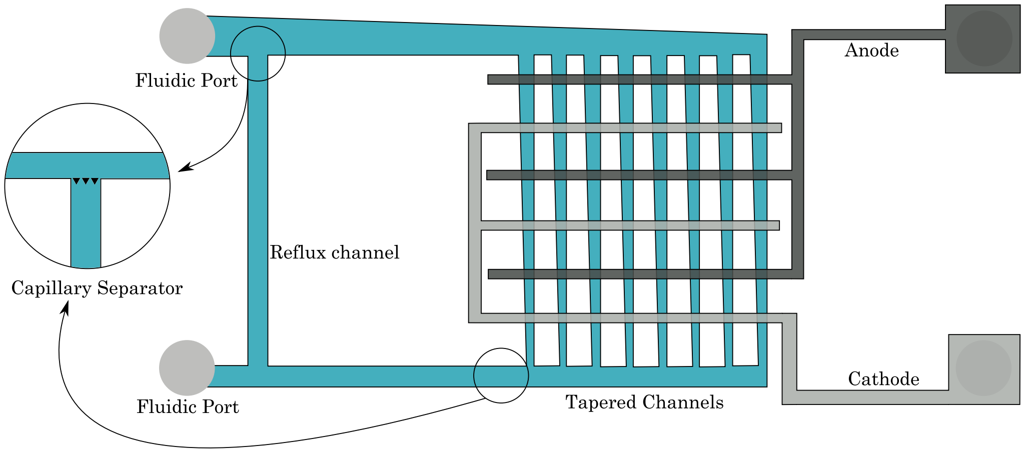

Figure 2.2: Sketch of the first generation chip design used to test various parts. The electrodes are explained in Chapter 2: Electrolysis of Water. The capillary separator and the tapered channels are discussed in Chapter 3: Gas Transport. This design will produce a mixture of hydrogen and oxygen, which are self-propelled to the outlet port. The chip will be filled with an electrolyte solution. The diameter of the channels are 300 µm to 600 µm wide and 50 µm deep.

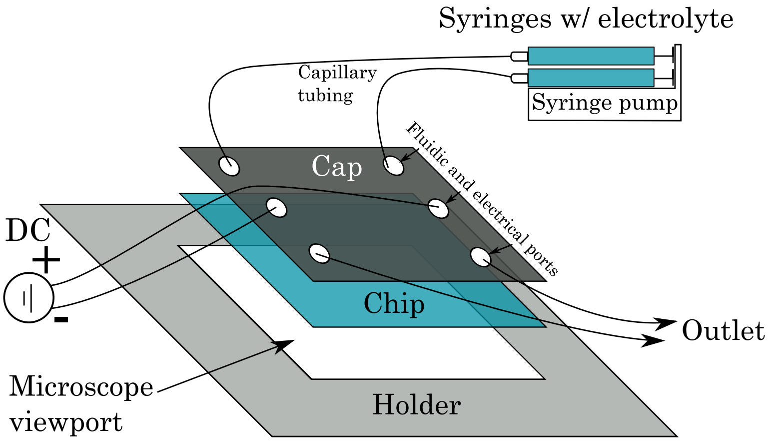

Figure 2.3: A sketch of the setup as used. The cap is clamped to the holder using screws to sandwich the chip inbetween. Upchurch connectors are used to connect the capillary tubing to the chip. The outlet fluid/gas mixture can be led into a container for further analysis. Optical measurements can be done by using the microscope viewport on the bottom of the chipholder.

2.3. Electrolysis: Results

After the two chip types were designed and produced, they were tested by filling them up with sodium sulfate solution and applying current. This process was filmed using an optical microscope (5x magnification). The goal of these measurements is to visually check if gas bubbles are formed when power is supplied to the system.

2.3.1. Indium tin oxide electrodes

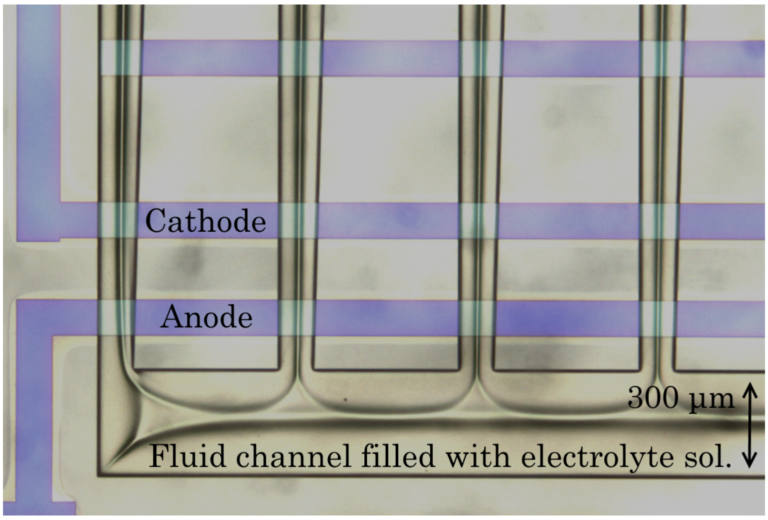

Figure 2.4: A microscope image of the chip filled with electrolyte before operation. This device uses the ITO electrodes, which are semi-transparent.

The first batch of measurements used the chips with ITO electrodes. In Fig. 2.4 a microscope image is seen of the chip before the power supply is switched on. It can be clearly seen that the ITO is transparent. After switching on the power supply (at 2.8 V DC), gas bubbles start to form as can be seen in Fig. 2.5(a). However, the electrodes also immediately got damaged during this operation. After flushing the gas it can be clearly seen in Fig. 2.5(b) that both the cathode and the anode are damaged. After this flush, power was again applied and the ITO being damaged was more carefully studied, as can be seen in Fig. 2.6. Over a short period of time, a significant amount of the remaining ITO is also removed from the chip's surface. This process was observed in three separate chips in total.

The reason for this removal of ITO is probably the formation of hydrogen ions at the anode, as explained in Eq. 2.1. These hydrogen ions can etch away the ITO, and this process is also observed in literature [13]. After flushing, the hydrogen ions are transported further along to etch away more of the ITO. After these measurements it was decided that ITO is not useful to implement as electrode material in the final design of the chip.

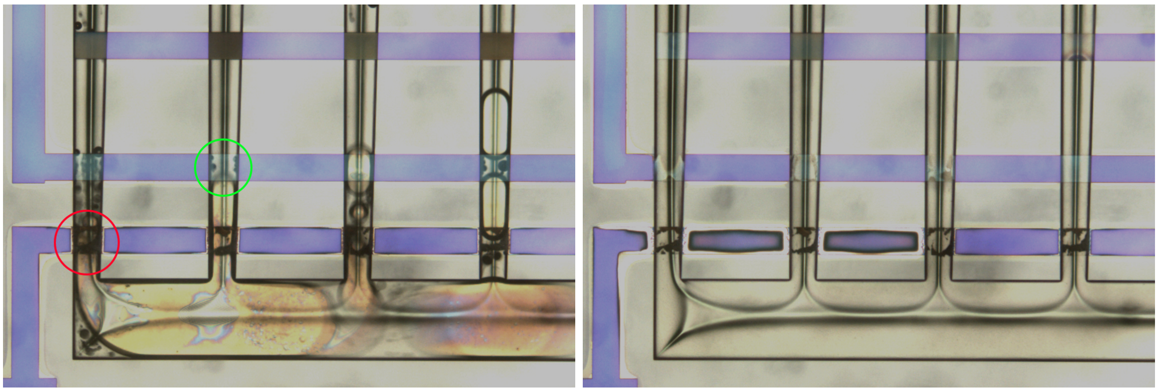

(a) (b)

Figure 2.5: *(a):* A microscope image during operation. A current of 2.8 V was applied to the electrodes to produce the gas visible in the image (rainbow colored parts). Damage to the electrodes is already visible, as marked with the colored circles. Note that the anode is more damaged compared to the cathode. *(b):* After flushing the system, a new image was taken to observe the damage to the electrodes. Note that both the cathode and the anode are damaged.

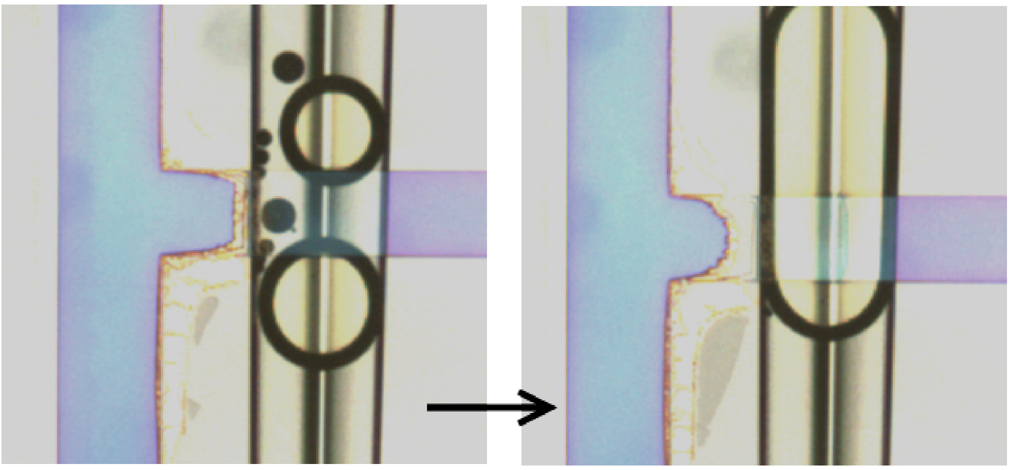

Figure 2.6: Two microscope images taken 30 seconds apart of the chip while producing gas. The removal of ITO over time is clearly visible.

2.3.2. Platinum electrodes

After noticing the failure of the ITO electrodes, chips with Pt electrodes were tested under the same circumstances. Fig. 2.7(a) shows the chip filled with sodium sulfate solution before operation. In contrast with before, these electrodes are not transparent. After switching on the power supply at 2.8 V, bubbles again start to form. However, the Pt electrodes are not etched away by the acid, and gas keeps being produced for prolonged periods of time (over 5 min). After operation and flushing, the electrodes have suffered no visible damage. Multiple measurements were performed on multiple different chips, all leading to the same results. These measurements were considered to be a success, and therefore for the electrodes in the final design Pt will be used as the material.

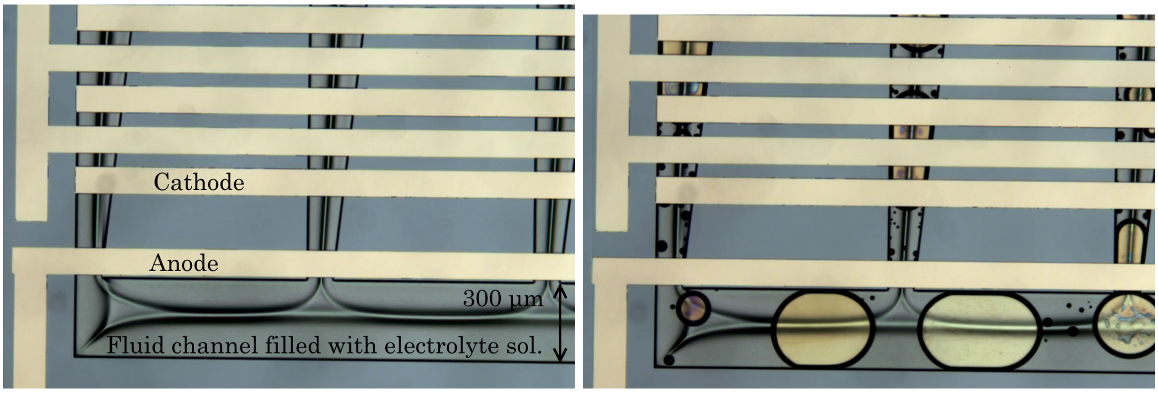

(a) (b)

Figure 2.7: *(a):* A microscope image of the chip with Pt electrodes before operation, filled with sodium sulfate solution. Note that the electrodes are not transparent. *(b):* When a voltage of 2.8 V is applied, gas starts to form inside the chip. After flushing, no damage is visible to the electrodes.

3. Gas Transport

Besides producing hydrogen on a microchip, the gases also need to be transported to a storage container. In large-scale systems this could for instance be done by letting the gas bubble out of the solution. However, in a micro-scale system this is more difficult. It is possible to pump out the mixture of water and gas, but this process leads to an energy loss. In this chapter alternative methods for gas transport are investigated. Besides transporting gas to a certain location, methods of blocking gas streams in microfluidic channels are also investigated.

3.1. Gas Transport: Theoretical Background

As hydrogen is produced by electrolysis, gas bubbles will form on the anode and cathode. This process is further explained in Chapter 2: Electrolysis of Water. As the bubbles grown on the electrodes, they prevent further liquid from contacting the surface, and thus blocking production of more gas. This means the gas needs to be removed from the electrodes as soon as possible. Conventional methods include using buoyancy to let the gas float away, and using a fluidic pump to flush out the gaseous stream [14]. However, these methods are either not usable in microfluidic systems or cost a significant amount of energy. Because this system is microfluidic in nature, capillary forces will keep the gas bubbles attached to the walls of the fluidic channel and the electrode surface, so external forces are needed to transport the produced gas away from the electrode surface.

A novel method to transport produced gas on microchips has been investigated by Paust, Metz et al [14][15][16]. It is proven that tapered capillary channels can produce the necessary pumping action without needing any external power. This method of passive pumping is further explored in subsection 3.1.1, and will be incorporated into the final chip design.

Besides moving the gas from the electrodes to the outlet, it is also necessary to keep the gas out of parts of the system, like the inlets. This is both a performance and a safety issue. If the gas can go to the wrong in- or outlet, it is lost and thus decreases the overall performance of the system. If hydrogen escapes and comes into contact with oxygen, it forms a highly combustible mixture that can lead to dangerous situations. Therefore it is imperative that a system is designed that acts as a barrier to gas, but can let fluids through. This is further discussed in subsection 3.1.2.

3.1.1. Tapered channels

Tapered channels are fluidic channels where one of the walls is at an angle to the other. This creates a difference in channel width along the length of the channel, which leads to self-propelled movements of growing bubbles. The detailed workings of this phenomenon are explained in this subsection.

All curved interfaces have a pressure difference between the inside and outside of the interface. This pressure difference is called Laplace pressure, and it is a result of a difference in surface tension between a liquid and a gas, or two immiscible liquids. The value of this pressure difference is determined by the Young-Laplace equation, shown as Eq. 3.1 [14]. As can be seen from Eq. 3.1, if the surface tension γ is constant, the pressure difference is a only a function of the radii of curvature in the width and height of channel R_w and R_h.

$$\Delta P \equiv P_L \equiv P_{inside} - P_{outside} = \gamma(\frac{1}{R_w} + \frac{1}{R_h}) \tag{3.1}$$

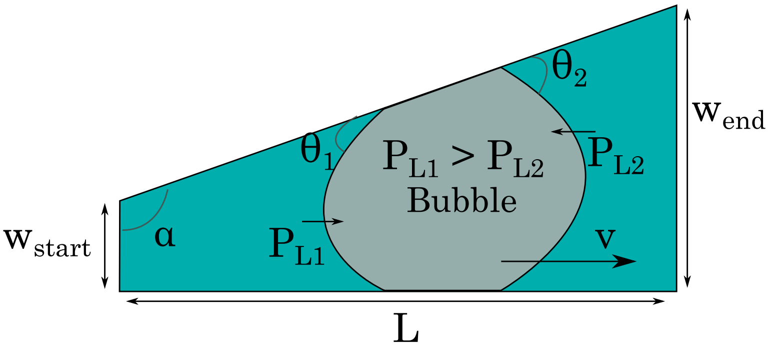

Figure 3.1: Sketch of a bubble inside a tapered channel. The Laplace pressure on the less wide bubble-water interface will be larger compared to the interface on the other side of the bubble. This leads to a movement in the direction of increasing channel width.

This means that as the radius of curvature decreases the pressure difference across the interface will increase, leading to a higher pressure inside a bubble compared to the atmospheric pressure around it. If a bubble is spherical, this pressure is equally distributed across the volume of the sphere. However, if a bubble is deformed in such a way that the width of the bubble is larger one one side compared to the other side of the bubble, a pressure difference along the bubble will form. The pressure on the smaller side of the bubble will be higher, leading to the bubble moving in the direction of the larger side. Another way to explain this phenomenon is by describing the free energy of the bubble surface. Any surface will eventually deform in such a way to reduce the free energy of the surface to a minimum [15]. For a gas bubble, this is achieved by moving the surface in such a way to produce a spherical droplet. By pinning the bubble between tapered channels, the only way for a droplet to reach such a geometry is to move further into the direction of increasing tapering. This process is shown in Fig. 3.1. In this figure, the difference in channel width is achieved by using a tapered channel. To make a tapered channel, one of the channel walls will be made at an angle to the parallel of the other wall. The used angle can be anything between 0° to 360°, but for the purposes of this research angles between 1.5° to 3° are used, in accordance to the findings of Paust, Metz et al [14][15][16]. Besides moving the bubble itself, the movement will also displace the liquid present in the channel, which means the bubbles act as microfluidic pumps [14].

For detailed analysis, it is useful to calculate the pressures that are generated by the bubble interfaces. Using trigonometry, the Laplace pressure that is generated at an interface can be calculated if the width and height of the channel are known along with the contact angle of the interface with the walls of the channel. This is shown in Eq. 3.2, 3.3 and 3.4.

$$R_w \equiv -\frac{w}{2\cos\theta} \tag{3.2}$$

$$R_h \equiv -\frac{h}{2\cos\theta} \tag{3.3}$$

$$P_L = \gamma(-2\cos\theta)(\frac{1}{w} + \frac{1}{h}) \tag{3.4}$$

In the used microfluidic channels, the height is constant across the device. However, by using tapered channels, the width is not constant, which leads to a change in Laplace pressure. The pressure at a certain point in a tapered channel is a function of the position of the interface in the channel, denoted by x. At $x = 0$, the width of the channel is equal to w_{start} as denoted in Fig. 3.1. At $x = L$, the width of the channel is equal to w_{end}. Thus, a linear relationship between x and w can be derived, as shown in Eq. 3.5. This equation can be combined with Eq. 3.4 to derive Eq. 3.6, which can be used to calculate the Laplace pressure of an interface inside the tapered channel if the contact angle and position are known. This can be used to calculate the pressure difference along a bubble inside a tapered channel.

$$w \equiv \frac{w_{end} - w_{start}}{L} x + w_{start} \tag{3.5}$$

$$P_L = \gamma(-2\cos\theta)(\frac{1}{\frac{w_{end}-w_{start}}{L} x + w_{start}} + \frac{1}{h}) \tag{3.6}$$

These relationships were used to create an predictive model for the calculation of bubble velocities by Metz et al [15]. This analytical model was confirmed to predict experimental results within a margin of 5%. However, this model is only usable for a certain range of channel sizes, which precludes the use of this model for the purposes of this research. If this model is to be used for calculations it first needs to be empirically fitted to the device used in this research. Because no true analytical model or explanation for the movement of bubbles in tapered channels exists in literature [14][16], no theoretical calculations are available to corroborate eventual experimental results. That means that the results of this work will lean heavily to the qualitative side.

3.1.2. Capillary separator

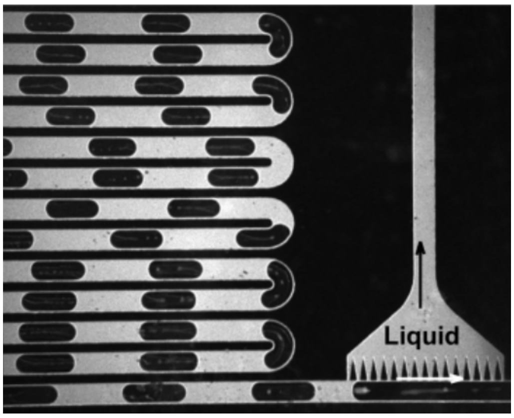

Figure 3.2: A microscope image of a capillary separator in action. As can be seen, only liquid passes through the row of 'shark's teeth' [17].

The system used will have gas bubbles in direct contact with liquid. The tapered channels discussed in Section 3.1.1: Tapered channels are used to move the bubbles in a certain direction, but this will also displace liquid to the exit point of the device. Thus there is also need for a method to separate gas from liquid in a microfluidic channel.

Gunther et al [17] describe a method of using tapered microchannels to separate gas from liquid in a microfluidic channel. Fig. 3.2 shows this so-called capillary separator. This device works by reversing

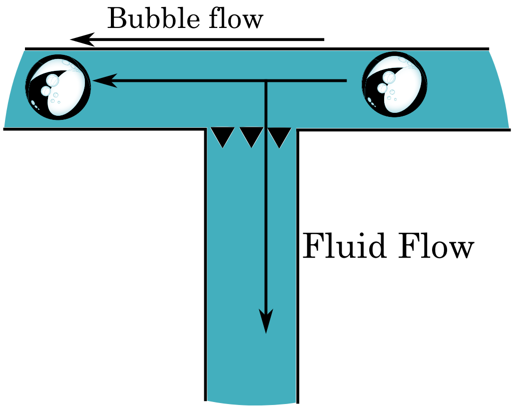

Figure 3.3: A sketch of the used capillary separator used to block bubble transport inside certain channels of the chip.

the principle used in the tapered channels. By creating channels with a small width, the Laplace pressure generated by gas inside these channels will be large (as explained in Section 3.1.1: Tapered channels). As this pressure needs to be overcome for gas to be able to move inside the small channels, this will create a barrier. The gas will move in the direction with the lowest resistance, and thus move past the capillary separator instead of through it. Liquid fills the channels, and can thus move through without creating an interface. By making the channel walls hydrophilic, water will have a lower resistance through the small channels compared to the main channel filled with gas. In this research capillary separators will be used to block off regions where gas is not wanted, as sketched in Fig. 3.3.

3.2. Gas Transport: Materials and Methods

As stated in chapter1, the goal of this part of the research is to find a method to transport gas using passive methods. At this stage the efficiency is not yet important, so the experiments focus on proof-of-concept data instead of measurement of variables.

The necessary structures were integrated into a chip that can also produce the gas needed to properly test the system. To test two research avenues in one design, the tapered channels and capillary separators were combined into the chip that was used to research the electrodes as discussed in Chapter 2: Electrolysis of Water, specifically Section 2.2: Electrolysis: Materials and Methods. An overview of the chip design is shown in Fig 2.2, which is reproduced on this page as Fig 3.4. A sketch of the overall setup is shown in Fig 2.3. The added parts are the tapered channels and capillary separators, which are discussed in the next paragraph.

The four parallel tapered channels used in this design all use an angle of 1.5°. The length of the channels is 4700 μm, a starting width of 100 μm and a final width of approximately 225 μm. These tapered channels exit into a larger tapered channel that leads to the outlet. The capillary separators are added to block off all exits except one for the generated gas. Their smallest width is the only important characteristic and is set to 10 μm. These dimensions were all chosen in accordance with the source material from Gunter et al [17] for the capillary separator and Paust et al [14][15][16]for the tapered channels, slightly modified to fit commonly used designs at Mesoscale Chemical Systems, University Twente.

As concluded in Section 2.3: Electrolysis: Results, platinum electrodes work properly for bubble generation, so they will also be used to generate the gas needed to test the tapered channels and the capillary separators.

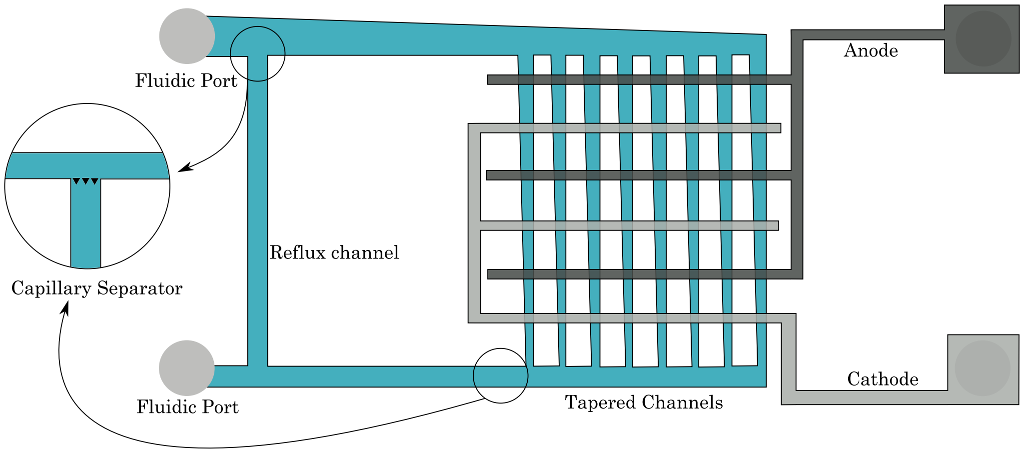

Figure 3.4: Sketch of the first generation chip design used to test various parts. The electrodes are explained in chapter 2. The capillary separator and the tapered channels are discussed in chapter 3. This design will produce a mixture of hydrogen and oxygen, which are self-propelled to the outlet port. The chip will be filled with an electrolyte solution. The diameter of the channels are 300 µm to 600 µm wide and 50 µm deep.

The device will be used to do a proof-of-concept measurement: to see if the formed bubbles move towards the exit, and to see if the capillary separator will block gas from moving across it. The chips were filled up with 1 mol/l sodium sulfate solution and a power supply was connected and run at 2.8 V DC for the duration of the trials. During this experiment videos were made using the microscope (Leica, DMI5000M) combined with a digital camera (Leica, DFC300FX) which are analysed in section 3.3.

3.3. Gas Transport: Results

This section will first discuss the results in regard to tapered channels, and finish with the results in regard to the capillary separator. The results are all in the form of images cut from videos made of the same device that was used in Section 2.3.2: Platinum electrodes.

3.3.1. Tapered channels

Fig. 3.5 shows the formation of bubbles at the start of the tapered channels as current is supplied to the anode and cathode. As can be seen in the images, gas bubbles form by nucleation at certain sites, and as they grow larger they coalesce into larger bubbles. As also can be seen from Fig. 3.5, the bubbles do not yet move into the direction of the larger taper, but mainly expand into the inlet channel, which has a larger width compared to the start of the tapered channel.

Fig. 3.6 shows the larger end of the tapered channel after the system has been running for 2 minutes. As can be seen, a bubble-slug that completely blocks the channel has been formed. This slug is moving towards the exit in a partly self-propelled motion, and partly because the fluid is being pushed by other bubbles. The velocity of this bubble is around 175 $\mu m\,s^{-1}$, which was calculated by measuring the time and the distance the front of the interface traveled.

Fig. 3.7 shows a gas slug exiting the system. As can be seen, the gas only moves while blocking the channel. If fluid can move past it, the gas remains stationary. This image sequence shows that gas is

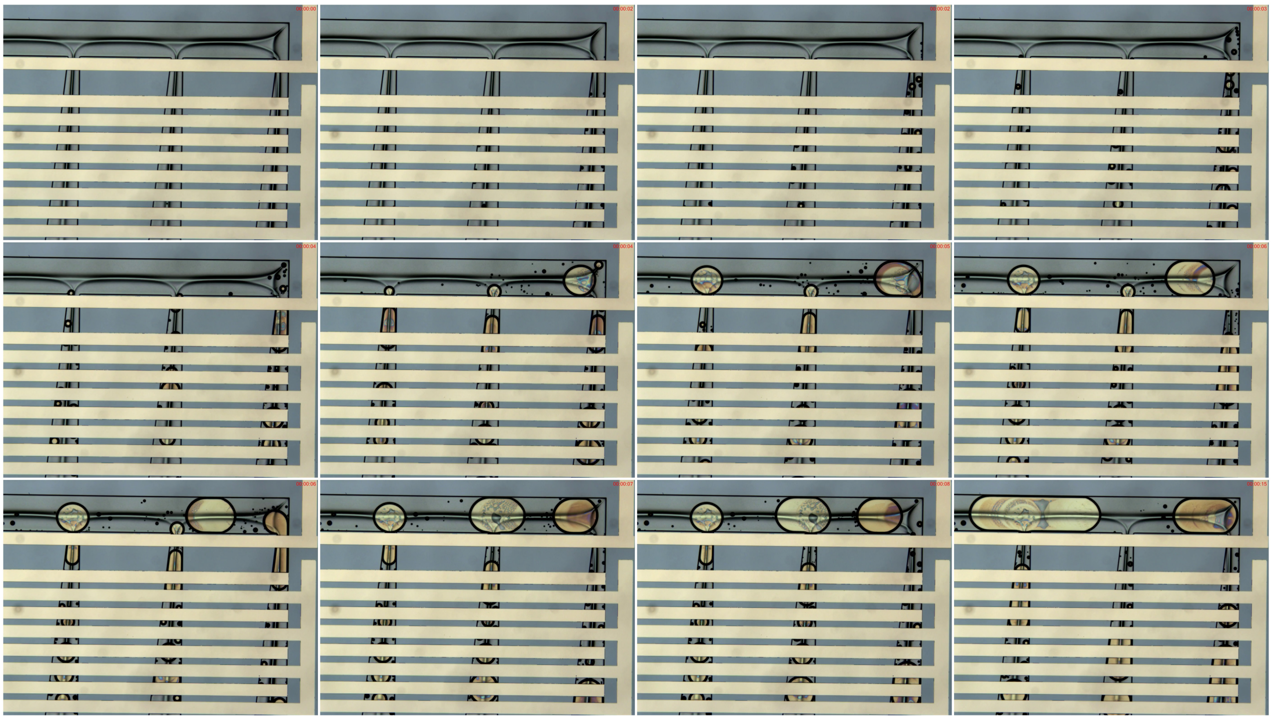

Figure 3.5: Image sequence left-to-right and then up-to-down with the first eight images 1 s apart showing gas formation after applying 2.8 V of DC current to the system. The final image (bottom right) is after 15 s of applying current.

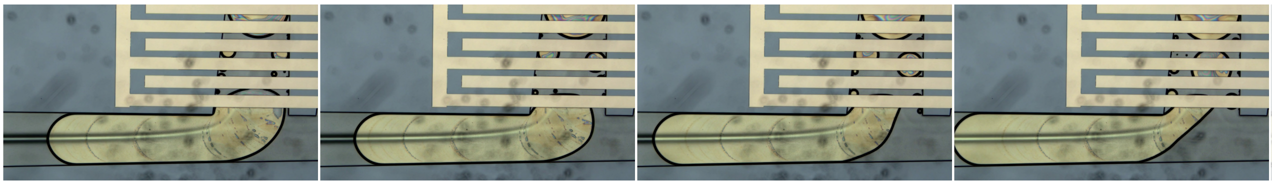

Figure 3.6: Image sequence with images 0.5 s apart showing a gas slug moving towards the exit of the system. The distance traveled by the leading interface of the slug in this time period is around 350 µm.

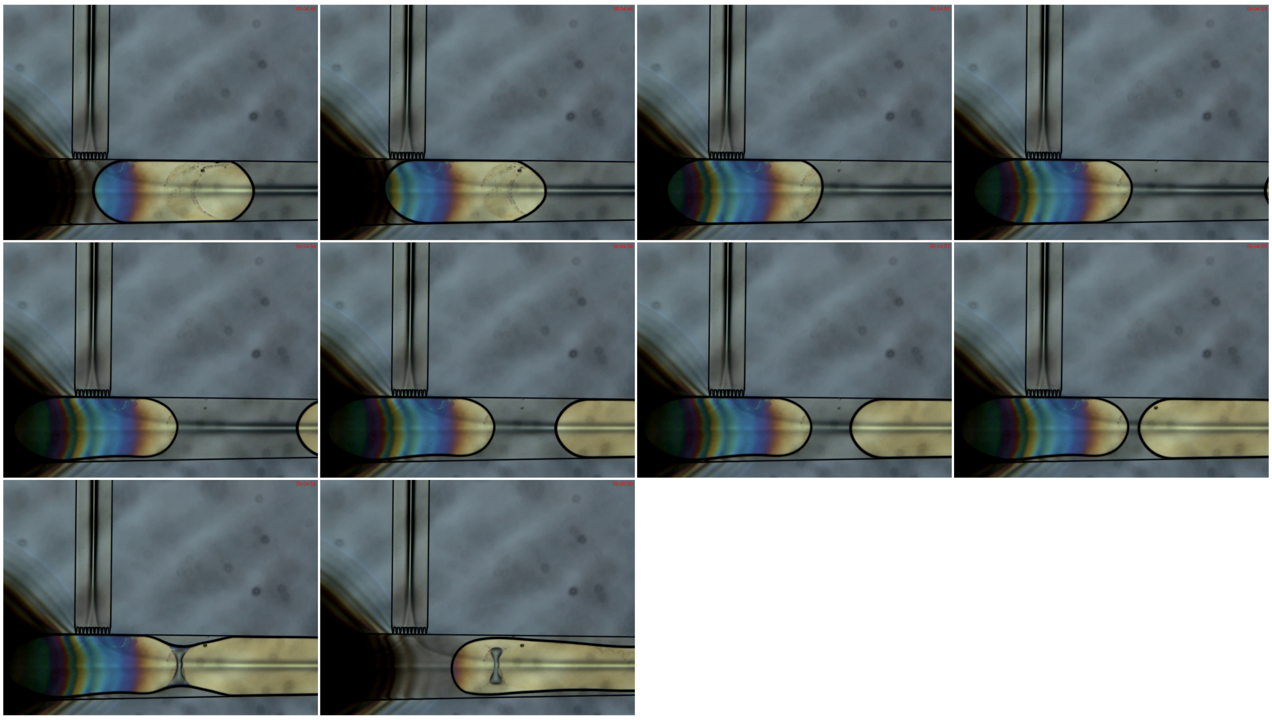

Figure 3.7: Image sequence during 14 s showing a gas slug exiting the system. The first slug moves while blocking the channel, but stops touching the bottom wall close the exit. Once the trailing slug coalesces with the first one, it pushes gas through the outlet port.

produced on the device, and afterwards it self-propels through the outlet port of the system without any external pumping.

These observations lead to the conclusion that the tapered channels work as expected. They ensure a movement of gas towards the outlet of the system. However, the gas that is produced in this system is a mixture of hydrogen and oxygen, as the cathode and anode are present in the same channel. In the final device these gases are produces separately. This might influence the contact angle, and thus the Laplace pressure, leading to a possible difference in self-propelling power of this design. However, the main parameter that influences the contact angle is the interaction between the liquid and the solid phase, with the gas phase having a minor role [18].

There are no large downsides to incorporating tapered channels in a electrolysis device. The channels lead to a passive movement of bubbles, and also decrease the chance of gas transport in the wrong direction. The only negative aspect is the increased complexity of designing a microfluidic device incorporating tapered channels compared to a design with parallel edges. This is especially true when considering the need to add a membrane, as will be explained in Chapter 5: Integrating & Combining.

3.3.2. Capillary separator

The working of the capillary separator can be seen in Fig. 3.7. The gas is completely blocked by the capillary separator, but fluid is still passing through. During the experiments, no gas was observed to travel through the capillary separators, thus it can be concluded that they work as expected. However, the small channels created by the capillary separator were also observed to be quickly blocked by any particles that get into the microfluidic device. This will quickly lead to a complete blockage of the channels. These blockages are very difficult to flush out once in place. In this phase of the research the added risks of this structure are larger than the possible positive effects. Therefore it was decided to not incorporate this structure in the final designs of this research.

4. Proton Transport

In Chapter 2: Electrolysis of Water, the process of producing gas from water is explored. However, in the methods used in that chapter the produced gas is a mixture of oxygen and hydrogen. As mentioned in Chapter 1: Introduction, it is important to keep the produced hydrogen and oxygen separated. If they are mixed they form an explosive mixture, and the gases are difficult to separate. To keep the gases separated while still allowing proton transport to take place, a proton exchange membrane is used. In this chapter a background on membranes is given, followed by a method to test which one is preferable for the purposes of this project. The chapter will not contain any experimental results, as the membranes need to be integrated with electrodes to properly test them. This will be further investigated in Chapter 5: Integrating & Combining.

4.1. Proton Transport: Theoretical Background

A membrane is a selective barrier that allows passage of certain chemical species, but blocks others. There are multiple ways of accomplishing this separating effect. The most basic form is the use of a molecular sieve: a porous structure that has holes of a few angstroms wide so only molecules smaller than a certain threshold can pass. Other membranes work by chemical interaction; for instance a membrane can be covered in polar or ionic groups which will heavily promote the passage of ionic particles, and block non-ionic particles.

In this project, the membrane should conduct only protons, and block the transport of hydrogen and oxygen gas. It does not matter if water is transported through the membrane. The protons are positive ions, so a negatively charged membrane surface should give a high selectivity towards them.

By using a membrane, the electrodes used for electrolysis can be placed much closer together without the produced gases mixing. This is shown schematically in Fig. 4.1.

4.1.1. Nafion

The most commonly used proton conducting membrane for electrolyzing purposes is Nafion, a fluoropolymer [19]. This material consists of a tetrafluorethene backbone that is functionalized with sulfonate groups. While the backbone is non-polar and thus does not conduct protons, the sulfonate groups are able to absorb and release protons. The backbone provides a solid platform for these groups and makes Nafion thermally and chemically stable [20]. Nafion's structure also adds to the membrane's proton transport properties. The membrane consists of a network of pores which are lined with sulfonated groups. A schematic depiction of this structure is shown in Fig. 4.2(a). The pores are completely filled with water, but these molecules will not enter the hydrophobic backbone.

The proton transport in such a membrane can take place in three different ways. All three methods are schematically depicted in Fig. 4.2(b) The most basic and slow mechanism is the bulk mass diffusion of protons through the water. In this mechanism, protons physically move through the liquid. This transport is limited by the diffusion rate of protons through the liquid. The second method is proton transport through

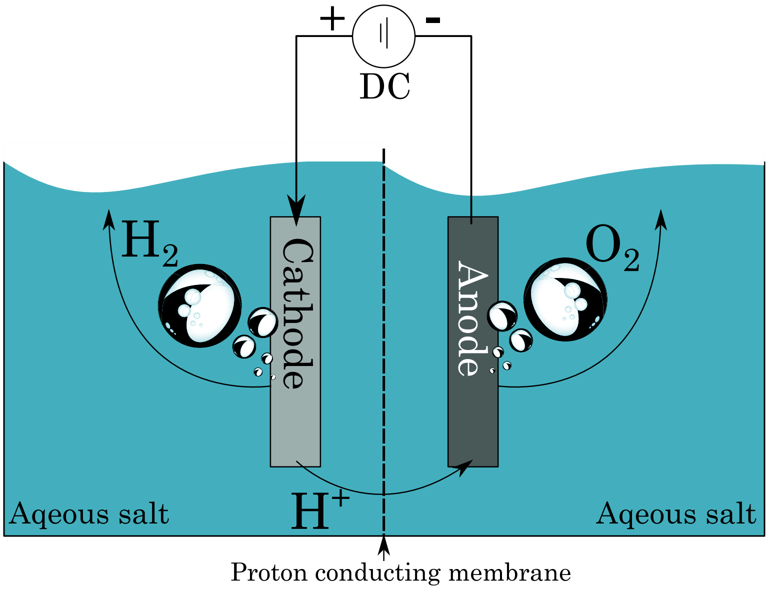

Figure 4.1: Electrolysis of water using a proton-conducting membrane, shown here as a dotted line. The membrane only lets protons through and blocks the formed gases. The electrodes can be placed anywhere on opposing sides of the membrane.

the surface of the membrane. In this mechanism, protons hop from sulfonic group via water to a new sulfonic group. These groups are attached to the surface of the nafion. As this transport only takes place on the surface, the transport velocity is relatively low. The final method is proton hopping through the bulk water, called the Grotthuss mechanism. This mechanism works by letting the proton absorb on a water molecule, forming a H_3O^+ group. This group will cluster with normal water molecules in the presence of a Nafion surface, and the positive charge can hop between the molecules to the other side. Grotthuss explained this effect using a bucket line as an analogue: imagine a row of people passing along buckets of water. As soon as a bucket is transferred to the next person, a new one is received from the other side. As this transfers mainly charge and reduces the length of mass transport this mechanism is very quick compared to the others, in the order of 4 magnitudes faster compared to bulk diffusion and 100 times as fast compared to surface diffusion [21].

As the Grotthuss mechanism is by far the fastest acting mechanism of proton transport, circumstances in and around the membrane should be calibrated to achieve the correct circumstances for this type of transport. This means the membrane should be fully wetted at all times, and the width of membrane pores should be in the order of 4-6 nm [21]. The surface of the membrane should also behave as an acid to promote the forming of the water clusters.

Chinen et al [22] proved that as the size of membrane pores decreases, the proton transport increases, as shown in Fig. 4.3. This increase in diffusion is most likely caused by a more efficient Grotthuss mechanism in small pores, due to the stronger alignment and clustering of the water molecules. As this pore size is thus one of the most important aspects of the membrane when looking at proton transport, different membrane types can be considered as long as they contain active groups on the surface and small nanochannels are formed. One such membrane type is porous silicon, which is explained further in Section 4.1.2: Porous silicon.

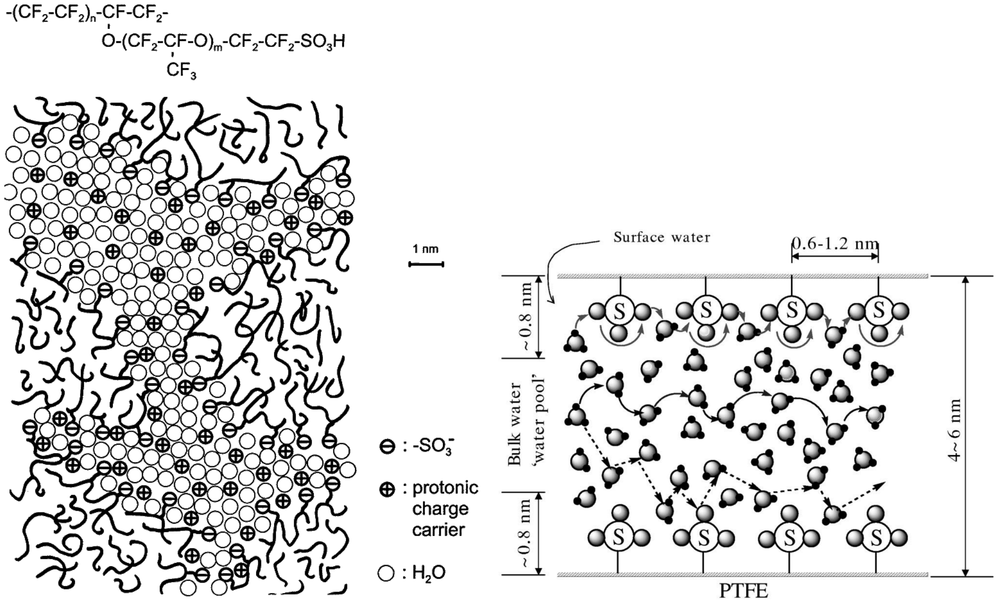

(a) (b)

Figure 4.2: *(a):* Schematic view of the structure of a Nafion membrane [20]. The lines depict the apolar backbone of the Nafion. The chemical formula of the membrane is shown above the structure. *(b):* Sketch of the three main mechanisms of proton transport inside a Nafion membrane [21]. The Grotthuss mechanism is depicted by dotted arrows, bulk diffusion by full arrows, and surface diffusion by the lighter arrows.

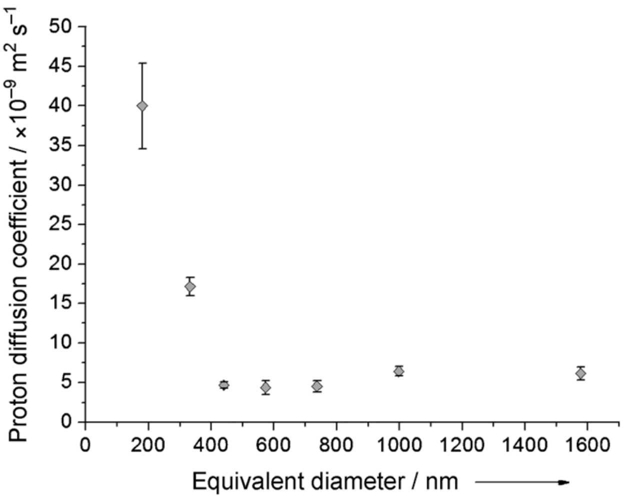

Figure 4.3: A plot of the proton diffusion coefficient compared to nanochannel diameter [22]. As can be seen, the diffusion of protons increases greatly if the pore size decreases. The Grotthuss mechanism might explain this behavior.

4.1.2. Porous silicon

Porous silicon consists of a silicon substrate that is riddled with small pores to form a network. It can be produced in multiple ways, but the most common one is the anodization of a silicon wafer in a HF solution [23][24]. The pores of this structure are lined with Si-OH groups which can perform the same aligning of water molecules as Nafion does using the sulfonate groups. These Si-OH groups can also be replaced with other functional groups to change the surface behavior of the membrane [23].

The porous silicon is created by electrochemically etching a p^{++} doped silicon wafer with HF. The redox reaction that takes place at the cathode (usually a platinum counter electrode submerged in the HF) is shown in Eq. 4.1, and the reduction that takes place at the silicon surface is shown in Eq. 4.2. In this reaction, h^+ are holes in the silicon valence band that are used as oxidation equivalents [25]. During the etching of silicon, the formation of pores starts perpendicular to the surface of the silicon wafer, and will follow the electrical field lines between the anode and the cathode. By making sure these lines are parallel to the surface of the wafer, horizontal pores can be created throughout the membrane. By controlling the etching time the depth of these pores can be controlled [26].

$$2\,H^+ + 2\,e^- \longrightarrow H_2 \tag{4.1}$$

$$Si + 6\,F^- + 2\,H^+\,2\,h^+ \longrightarrow {SiF_6}^{2-} + H_2 \tag{4.2}$$

As shown in Fig. 4.3, if the pore size of the membrane is reduced, proton transport increases [22]. Because anodization of silicon can be precisely controlled, it is possible to create very small nanochannels to be used as a membrane. Another advantage of using this type of membrane is the ease of integrating it into a microfluidic chip; as most common microchips are already made out of silicon, the membrane can be produced by anodizing the wafer after etching the channels.

4.2. Proton Transport: Materials and Methods

To be able to correctly test these devices they need to be integrated into a design that can produce protons. This means electrodes need to be placed on the chips. The details of the used electrodes are discussed in Chapter 2: Electrolysis of Water. Because the electrodes need to be integrated in a design with the membrane to properly test the usage during electrolysis, tests need to be conducted by integrating them both into a single design, which is further discussed in Chapter 5: Integrating & Combining. This research features no trials done with the two membrane types without using electrolysis. However, tests with membranes were done by the research group Mesoscale Chemical Systems at the University Twente as part of the larger project as outlined in Chapter 1: Introduction. The tests were performed by applying either a chemical or an electrical potential across the membrane to see the effects. This is shortly explained in subsection 4.2.1.

To compare the membranes identical chip designs are used, with the only variable being the membrane type. Because of inherent production limitations of the membranes, these two chip types are produced differently. The details of producing chips containing these membranes will be discussed for each membrane type in subsections 4.2.2 and 4.2.3.

4.2.1. Characterizing Membranes

Once the membranes are produced and integrated into a system, they can be evaluated to determine their effectiveness. There are multiple parameters that govern the proton transport through a membrane, including pore size as outlined in Fig. 4.3, electrochemical potential, wetting, porosity, conductivity and more. The most straight-forward method of characterizing the membrane is by measuring the current across the membrane when a voltage is applied. By varying the voltage, a relation between current and voltage can be obtained. The slope of the resulting line equals the conductivity of the system. These measurements can be conducted by using a potentiostat. Usually a potentiostat will a three-electrode system for measuring: an anode, a cathode and a counter-electrode that supplies the power. However, by using microfluidic chips the channels are not directly accessible and there is no room for bulky electrodes. There are two options to circumvent this problem: integrate measurement electrodes inside the chip, or measure at the outlet. Measuring at the outlet introduces a large error, as the path length of the system will differ every time, depending on the length of the connection and channels. Integrating electrodes requires a specific design, which further complicates matters. Previous research at Mesoscale Chemical Systems on characterizing membranes has used the outlet-method of measuring. The integration of electrodes on the chip as outlined in Chapter 5: Integrating & Combining gives a possibility of measuring using electrodes embedded in the chip, which will possibly lead to a reduction of measurement errors. The membranes will not be characterized as part of this project, as this is not an aim of the current work. However, once a design has been produced and proven to work, one of the next steps will be to determine the effectiveness of the proton transport through the membrane.

4.2.2. Nafion-based design

Nafion is not easily integrated in conventional microfluidic chip production techniques. This means that the Nafion layer needs to be added to the chips after the production. In order to achieve this, the produced chips intended for use with Nafion are not bonded in the clean-room, but produced as two halves: a cap and a bottom. The Nafion will be sandwiched between these layers to act as a proton-conducting layer.

The Nafion is semi-transparent, but not enough to accurately see the fluidic channels through it using microscopy. This means the channels themselves need to be made in transparent material. This is achieved by depositing a SU-8 (an epoxy-based photoresist material) layer on top of a glass slide that contain the platinum electrodes, followed by producing channels in this polymer layer. Producing channels is done by selectively curing the SU-8 using a mask and UV-light, followed by washing away the non-cured regions. The electrodes need to be in the channel layer in order to facilitate the electrolysis. They will also block visual access to the chip, but all parts that are not covered by electrodes can be seen through the glass and SU-8. The Nafion can be cut to size and clamped between the SU-8/glass layer and the glass cap.

Once the parts are clamped together, the membrane can be tested and characterized. As producing this chip needs to contain electrodes, a membrane and a method for gas transport, the results of these test are discussed in Chapter 5: Integrating & Combining.

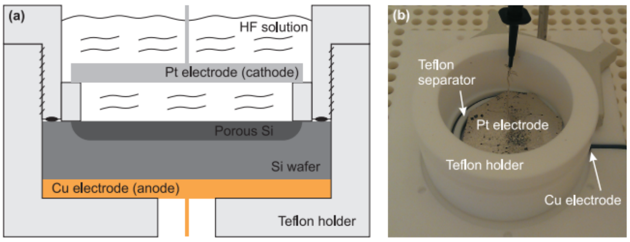

Figure 4.4: A sketch (a) and a photograph (b) of the anodization chamber used to create the porous silicon membrane on a silicon wafer. [26]

4.2.3. Porous silicon-based design

The porous silicon-based design has a large practical advantage of the Nafion-based design, as microfluidic chips are usually made from silicon. No additional material is needed to incorporate the membrane in a MFC, which vastly reduces production complexity. The set-up used to produce the porous membranes is depicted in Fig. 4.4. The details of the production process of the chips and membranes can be found in Chapter A: Production details. As explained in the previous section, a membrane by itself cannot be used: electrodes and tapered channels are also needed. The details of the chip that was used to test the membranes can be found in Chapter 5: Integrating & Combining.

5. Integrating & Combining

In this chapter the results of the previous work is combined into a final testing device that can be used to do research into electrolysis of water on a microchip. In section 5.1 the design of the chip is explained, including all the different parts and why they were chosen. In section 5.2 descriptions of how the device is produced and experiments are done are given. This chapter concludes with the results in section 5.3.

5.1. Integration: Design Considerations

As explained in the previous chapters, there are multiple parts that need to be integrated into the final design. Chapter 2: Electrolysis of Water explains electrolysis and the electrodes that will be used in this device. The design will be different however. Instead of interdigital electrodes across the channels, the anode and cathode will cover parallel channels that are separated by a membrane as explained in Chapter 4: Proton Transport. The two membrane types that are detailed there will both be tested: Nafion and porous silicon.

In Chapter 3: Gas Transport two structures for passive manipulation of gas were investigated. The tapered channels are advantageous to integrate while having no obvious downsides, so they will also be integrated in this final design. The capillary separators lead to a high chance of blocking the channels, so they will not be used in this design in order to reduce operating complexity.

Combining these three parts will require a completely new design. There are several severe constraints because of the used materials and parts. Using a membrane necessitates parallel channels that cannot cross, and as the device will be made using lithography of silicon three dimensional structures are not possible to produce. The tapered channels need to continually increase in width, or the working of the channel is lost. The electrodes are also not allowed to touch each other, and the anode cannot cross over channels that are connected to the cathode and vice-versa. The substrate they are on needs to be electrically isolated to prevent shorting out the system.

After testing the individual components, the following design choices were made for the final design:

Electrodes	The electrodes are needed to electrolyze the water into elemental oxygen and hydrogen. Platinum electrodes were chosen for this design, as they function as a catalyst, conducting surface, are highly resistant to corrosion and are easily implemented into the production process. The main downsides of using platinum as electrode material are the costs and the opaqueness of the material. For these experiments those are minor concerns.
Channels	The channels carrying the fluids are electrochemically etched in the silicon wafer, or constructed using SU-8 on a glass wafer. The channels are 10 µm deep, just as in previous iterations. The channel width is not constant but increases along the length of the channel, as they are tapered. The angle of tapering is variable, but will be kept between 1.5° to 3°, as tested in earlier designs. To incorporate the membrane, two parallel channels are used. To optimally use the available surface area of the chips, the channel will have a serpentine

geometry. The capillary separators as tested will not be integrated in this design in order to reduce possible failure points due to blockage of the channel.

Membranes Two membranes will be tested: Nafion and porous silicon. The details of these membranes are outlined in Chapter 4: Proton Transport. Nafion cannot be integrated in the chip during regular production, so the constituent parts are made and clamped together to perform measurements. The porous silicon is made by electrochemical etching of the wafer after the channels are produced.

By combining the lessons learned from previous iterations, a final design was proposed. A sketch of the system is proved in Fig. 5.1. This sketch shows the system with a porous silicon membrane. A Nafion membrane cannot be integrated between the channels but is instead clamped on top, with SU-8 functioning as a separating wall between the two channels. This leads to a design with two parallel channels that are both continually increasing in width, but with a constant distance between them containing the membrane. The electrodes should cover the fluidic channels; one channel covered by the anode and one covered by the cathode. In order to increase the used space on the device, the channels will not be straight but serpentine to cover a larger area. To accomplish all this, a MATLAB-code will be written to generate these intricate structures.

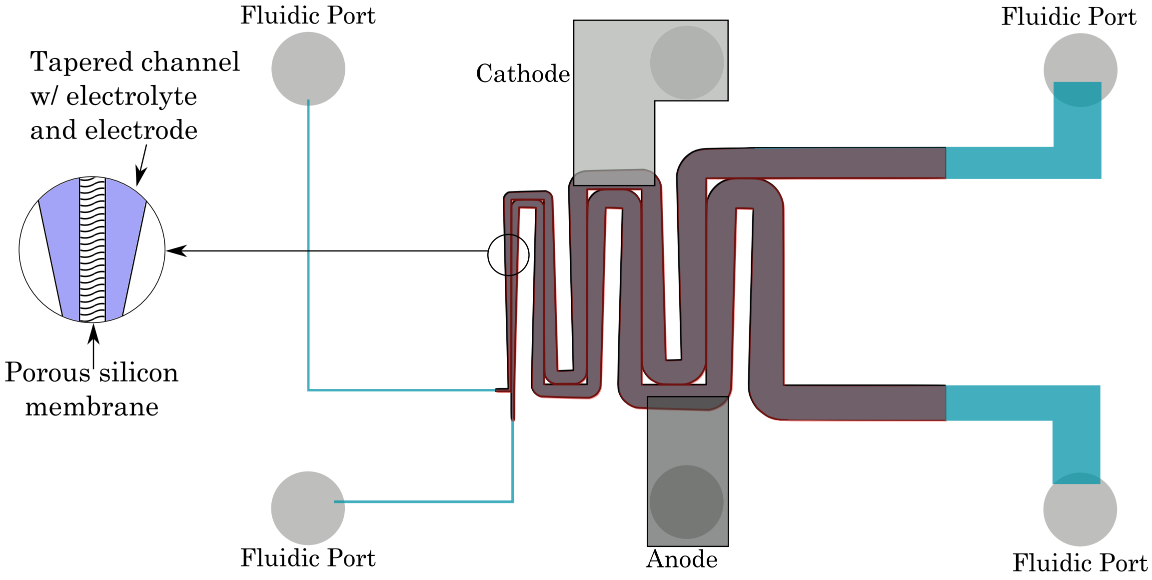

Figure 5.1: Sketch of a second generation chip design used to test various parts. The electrodes are explained in Chapter 2: Electrolysis of Water. The anode covers the grey part of the top channel, and the anode the grey part of the bottom channel. The tapered channels are discussed in Chapter 3: Gas Transport. The details of the membrane are explained in Chapter 4: Proton Transport. This design will produce two separated streams, one containing oxygen and one containing hydrogen. Both are self-propelled to the outlet port by the working of the tapered channel. The chip will be filled with an electrolyte solution. The amount of windings of the channel and the angle of tapering are variable, thus leading to a variable width of the channel. The inlet channels are 100 µm wide, and all channels are 10 µm deep. The width of the membrane is 10 µm between straight parts of the channel, and variable in the corners.

5.2. Integration: Materials and Methods

The chips were designed in Clewin 5 (PhoeniX Software) using Matlab-code to construct the tapered channels. The code is detailed in Chapter B: Matlab Scripts. The code is parametrized, and as such an infinite amount of designs can be made from it. The chose parameters are listed in the table below, and a sketch is provided in Fig. 5.1.

Parameter	**Value**
Starting channel width	100 µm
Ending channel width	1000 µm
Channel depth	10 µm
Membrane thickness	10 µm
Tapering angle	3°

The platinum electrodes have the exact same dimensions as the channels, but a band of 3 µm on the outsides is not deposited to make sure the platinum does not touch the membrane surface and/or the other electrode. For the silicon-membrane based design, the channels are produced by plasma-etching a silicon wafer using a mask based on the Clewin-design. The details of this process are provided in earlier chapters. After etching the channels, through holes are added on 6 places as shown in the sketch. Four of these function as fluidic access ports, and two are used to make electrical connections. The silicon membrane is produced after this step. The details are explained in Chapter 4. The glass slide that caps off the silicon channels is etched back 100nm on places where the platinum will sit, and the titanium is then sputtered on top of that. The glass slide is then anodically bonded to the silicon chip to cap it. The wafer is then diced into individual 10x20 mm chips. To make an electrical connection, the through-holes that lead to the anode and cathode are filled with 2-part silver epoxy (MG Chemicals,U.S) , along with an electrical wire. The channels are filled with an electrolyte, 5 mmol/l sodium sulfate solution. An external power supply was used to connect the wires and perform the electrolysis. A potentiostat (Palmsense, Palm Instruments) was used to perform basic electrical measurements.

For the Nafion-based design, the chips were made out of two glass slides. The top part is a clear glass slide. The bottom part contains the walls, which were built up using SU-8, and the electrodes which were sputtered onto the glass. The Nafion was purchased as a sheet, cut to size, and was prepared as instructed by soaking it in water for a few hours. To use the chips, the Nafion was clamped between the top and bottom glass slides.

As the microchips only contain a single set of electrodes, electrical measurements to characterize the membrane are not easily done. By filling the two channels with solutions with different pH's, protons will travel through the membrane because which can be measured by using the available electrodes. On earlier prototypes the results of these type of measurements were not consistent with the theory, and were difficult to accomplish. Reports of these experiments can be found in Chapter C: Porous silicon membrane experiments. On the basis of these reports it was decided to not continue with these types of measurements in the final experiments. The main difficulty with obtaining data is the fact that only one electrode is available in the device, which has to perform two roles to be able to measure electrical resistance: producing gas by electrolysis and measuring current through the electrode. These measurements are therefore not possible to perform with the current design.

To determine if the tapered channels and membrane perform as expected, the chip is first filled with the mentioned sodium sulfate solution. Then all external fluidic sources are decoupled to ensure all movement is strictly due to the formation and movement of the gas bubbles that are produced in the device. The electrical leads are connected to a power supply, and the voltage is increased until bubbles form. Because the electrodes are opaque, the microscope will be aimed at the outlet channel. If the device works as expected, all bubbles will move towards the through holes at the end of the channels. The images are later analyzed using software. If clear images are obtained, the volume and movement speed of the produced gas can be calculated from the images as all dimensions are known.

5.3. Integration: Results

The produced chips were prepared for measurement by filling the chip with elecrolyte and applying a power to the electrodes until gas formation at the outlet was visually confirmed by microscopy. The Nafion-based design produced no succesful results. Clamping the Nafion membrane and glass slide to the SU-8 patterned chip proved to be difficult to do without creating leaks. The chip was submerged in the electrolyte solution and clamped while still submerged to fully fill all channels, but upon visual inspection it was clear the electrolyte would not stay inside the channels. A current was run through the electrodes, but the produced gas escaped from all sides of the chip.

It was decided to stop all experiments with the Nafion membrane using this design, as it was deemed experimentally impossible to close all the gaps evenly without breaking the glass on the chip. In Chapter 6: Discussion & Conclusion advice for possible future measurements using Nafion are discussed.

The porous-silicon based chips did produce results, which are discussed in the following paragraphs.

The chips were first filled with electrolyte by using syringes, upchurch connectors and a Harvard syringe pump. Both channels of the chips were completely flushed with the electrolyte solution for 30 minutes at a flow rate of 10 µl/min. After stopping the pump, the beginning and end of the channels were visually inspected for any left-over gas bubbles. If none were found, the syringes were removed and the chip was ready for measurements. If any gas was spotted, the flushing procedure would be repeated.

Once the chip was filled with electrolyte, electrical leads were attached to the silver-epoxy filled through-holes, and a steadily increasing current was applied using a power supply until gas was seen at the outlets of the system. However, no chips produced any gas. The chips were then used without using the silver-epoxy, instead clamping the wire straight the the platinum electrodes on the bottom of the through-holes. This method did result in gas formation, as shown in Fig. 5.2 and 5.3. As can be seen in the images, gas is only present in the channel containing the cathode. After a few more seconds, gas is also seen in the channel containing the anode, as shown in Fig. 5.4. A possible explanation of this observation is the fact that hydrogen gas is stoichiometrically produced at a rate double that of oxygen. The right channel produced the hydrogen (cathode side), and the left channel produced oxygen (anode side). As the power was increased until gas started to form, it is expected that the gas at the cathode will form much faster and thus will lead to earlier expelling of gas due to the tapered channel.

According to literature, the voltage at which electrolysis occurs in ideal circumstances would be 1.24 V, and previous experiments with inter-digital platinum electrodes showed a necessary current of 2.8 V for electrolysis to start. During the measurements on this device the necessary voltage was in the range of 2.8 V, and around 0.11 A which is similar to earlier experiments with inter-digital electrodes. This is a strong indicator that the membrane is not a limiting factor for proton transport. This will be further discussed in Chapter 6: Discussion & Conclusion.

Due to the difficulty in obtaining concrete and reproducible numerical results using this setup, no further data was obtained. Due to th difficulty in producing clear microscope images of gas movement, no analysis was done on the produced gas.

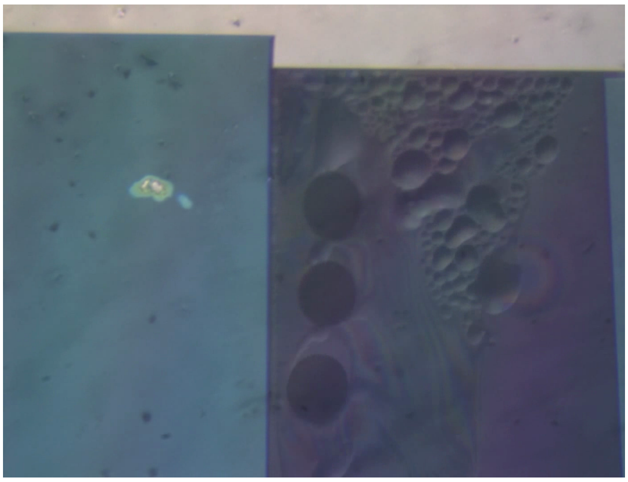

Figure 5.2: Gas formation in the final design. Only the cathode-side of the chip produced visible gas, and proper electrical connection was lost before any gas was detected in the anode-side of the chip. The movement of the gas is from top to bottom. It is also possible that the left-most channel was not completely filled with liquid, as the channel seems to have a different color compared to the right-most channel.

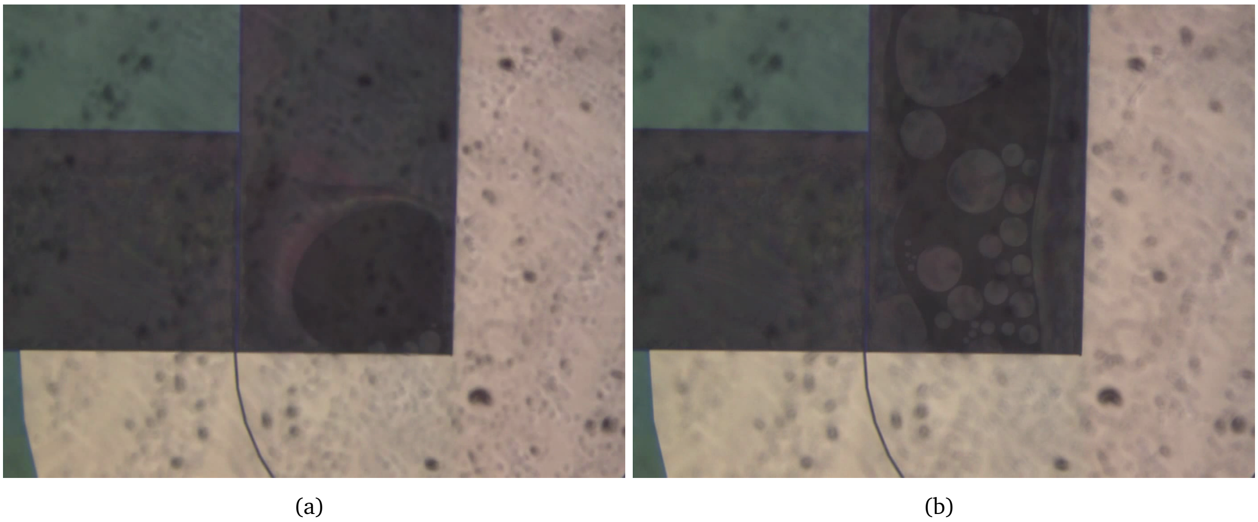

(a)

(b)

Figure 5.3: Two sequential frames captured with a digital microscope of gas formation in the final design using a porous silicon membrane. In this sequence gas formation can be seen in the left channel, which contains the cathode. The gas is expected to be hydrogen. Due to experimental problems the camera used was running on a low frame rate, and any detail between the two frames was lost. The movement of the gas is from bottom to top.

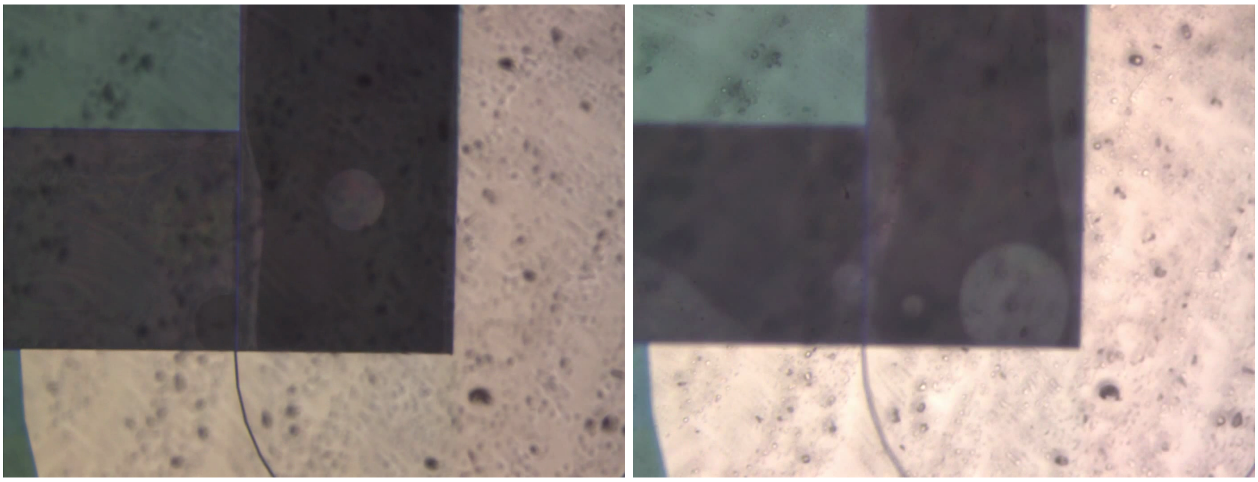

(a) (b)

Figure 5.4: Two non-sequential frames captured around 2 seconds apart with a digital microscope of gas formation in the final design using a porous silicon membrane. In this sequence gas formation can be seen in the both channels; a small bubble is visible in image *(a)*, and a large gas pocket is visible in image *(b)*. Image *(b)* is slightly out of focus due to movement of the chip underneath the microscope during the experiment.

6. Discussion & Conclusion

In this final chapter, the results of the work as outlined in the rest of this thesis are discussed, followed by concluding what was learned from the research, along with recommendations for future work.

6.1. Discussion

In this thesis, multiple parts that are necessary for the water-splitting reactor were designed and tested. In this section, each component will be discussed.

6.1.1. Electrodes

Electrodes are necessary for the electrolysis of water. However, during experiments it became clear that it would also be helpful it there was a second electrode in each channel to be able to perform electrical measurements. As these were not incorporated in the used designs, no useful electrical measurements could be done.

Two materials were tested as electrodes: indium tin oxide (ITO), and platinum. It was found that indium tin oxide was completely removed after performing electrolysis for a short period. The most logical explanation for this is the fact that during electrolysis acid is produced, and this can easily etch away the ITO thin film layer, as studie by Mammana et al for instance [27]. This means that pure and unprotected ITO should not be used as an electrode in this type of device, as proton ions will always form, and local concentrations can create sufficiently acidic conditions to effectuate electrolysis of the ITO. Platinum electrodes fared much better. Besides being resistant to electrolysis, platinum also functions as a catalyst for electrolysis of water. This catalyzing function can be improved further, for instance by adding a copper mono layer [28]. However, during trials no efficiency gains were observed between the use of ITO or platinum, as both needed a similar voltage before gas production started.

The only downside to using platinum is the opaqueness of the material. ITO is transparent, which is helpful during experiments. However, for the goals of this research it is possible to regard the device as a black box, and focus the research on the input and output. For optimization, less energy going in and more gas coming out are the main goals.

Finally, in the future the goal of this research is to not use electrodes for electrolysis, but incorporate an array of solar-powered electrolyzers inside the channels.

6.1.2. Channels

Two main channel geometries were tested during this research: tapered channels and capillary separators. The capillary separators were included in an earlier prototype and functioned as was described in literature: they effectively blocked all gas from moving through them, while no such obstruction was observed for liquid. If such a component is needed in a future device, this seems to be a no-frills solution.

The tapered channels also performed as expected. In early prototypes a clear movement in one direction was observed, and in the final design a large gas flow was seen exiting the system. However, no numerical data was obtained, and the shape of these channels is currently not optimized. As there seems to be no major downside to using tapered channels over straight channels apart from increased complexity in designing the devices, it is highly recommended to incorporate these tapered channels in all future electrolysis devices.

6.1.3. Membranes

Two types of membrane were tested in the final prototype: Nafion and porous silicon. Nafion was used mainly as it is one of the most used membranes in current research. However, no successful experiments were done using Nafion. As Nafion could not be integrated into the chips during production, it was sandwiched between layers just before the experiments were performed. This lead to a large amount of leaks, which precluded proper experiments. It was therefore decided to skip all Nafion experiments.

The porous silicon membranes were successfully integrated into the chips during production. Due to the high surface area of the used design, a large part of the chip was made porous, which led to problems during production. A significant amount of chips broke during production, and it was difficult to finally produce the device. This can be solved by reducing the open surface area of the device, for instance by not using a winding but a straight channel.

The silicon membrane was properly tested in the final device. During electrolysis experiments gas was observed to be produced in expected stoichiometric fractions. If the membrane did not conduct protons, no gas would form. If the membrane did not block gas from moving through, an equal amount of gas would form in both channels. It can therefore be stated that the membrane performed its task as expected. In Appendix C more experimental results can be found on the resistance of the membrane under differing conditions.

6.2. Conclusions & Recommendations

Although this research is far from finished, a number of conclusions and recommendations can be distilled from this work. The two main components of the final device were the tapered channels and the proton-conducting membrane.

For future water-splitting micro-reactor designs it is highly recommended to use tapered channels for the passive transport of bubbles. There are virtually no downsides to using these types of channels, but they have been proven to work in literature and experiments. This work does not provide any quantitative data on the effects of the tapered channels on the system.

Of the two tested membranes, porous silicon is preferable to use in the future. The main reason is the ease of production and integration of this membrane type compared to Nafion, but preliminary measurements and literature also show improved membrane characteristics of the porous silicon membrane compared to Nafion.

Besides these two main components, a number of auxiliary components were tested. During the research and characterization of these devices it is recommended to continue using platinum electrodes. A marked improvement would be to incorporate multiple electrodes in each channel to be able to perform electrical measurements during electrolysis. It is also recommended to design a different connection method instead of the used experimental set-up.

The capillary separator was successfully integrated in one of the earlier prototypes. Once a more final design is made, this structure can be used as a cost-effective and simple method for keeping gas bubbles out of certain parts of the device.

Finally, the most important recommendation is to decrease the complexity of the channels in order to simplify the design of the microchips, until more data has been gathered on the workings of all individual components. A suggestion would be to make a pair of parallel tapered channels without corners instead of the used winding set of channels. This would reduce the effectively used area of the device, but optimization should take a back seat until the influence of all parameters has been measured.

Bibliography

[1] G. M. Whitesides, "The origins and the future of microfluidics," *Nature*, vol. 442, pp. 368–373, July 2006.

[2] J. Ouellette, "A new wave of microfluidic devices," *The Industrial Physicist*, 2003.

[3] T. Riis and E. F. Hagen, "Hydrogen production r&d: Priorities and gaps." IEA, 2006.

[4] M. van Calmthout, "Eindelijk: zonnenaaldjes maken brandstof uit water," July 2015.

[5] M. A. Modestino and S. Haussener, "An integrated device view on photo-electrochemical solar-hydrogen generation," *Annual Review of Chemical and Biomolecular Engineering*, vol. 6, no. 1, p. null, 2015. PMID: 26083057.

[6] M. A. Modestino, K. A. Walczak, A. Berger, C. M. Evans, S. Haussener, C. Koval, J. S. Newman, J. W. Ager, and R. A. Segalman, "Robust production of purified h2 in a stable, self-regulating, and continuously operating solar fuel generator," *Energy Environ. Sci.*, vol. 7, pp. 297–301, 2014.

[7] D. Schroeder, *An introduction to thermal physics*. San Francisco, CA: Addison Wesley, 2000.

[8] J. Bockris and A. Reddy, *Modern Electrochemistry 1*. Kluwer Academic Publishers, 2002.

[9] A. Bard and L. Faulkner, *Electrochemical Methods: Fundamentals and Applications*. Wiley, 2000.

[10] Kitco, "Platinum price history," July 2015.

[11] H. Kim, C. M. Gilmore, A. PiquÃĺ, J. S. Horwitz, H. Mattoussi, H. Murata, Z. H. Kafafi, and D. B. Chrisey, "Electrical, optical, and structural properties of indiumâĂŞtinâĂŞoxide thin films for organic light-emitting devices," *Journal of Applied Physics*, vol. 86, no. 11, pp. 6451–6461, 1999.

[12] C. Belmont, R. Ferrigno, O. Leclerc, and H. Girault, "Coplanar interdigitated band electrodes for electrosynthesis. part 4: Application to sea water electrolysis," *Electrochimica Acta*, vol. 44, no. 4, pp. 597 – 603, 1998.

[13] S. Bashar, *Study of Indium Tin Oxide (ITO) for Novel Optoelectronic Devices*. Phd thesis, University of London, 1998.

[14] N. Paust, C. Litterst, T. Metz, M. Eck, C. Ziegler, R. Zengerle, and P. Koltay, "Capillary-driven pumping for passive degassing and fuel supply in direct methanol fuel cells," *Microfluidics and Nanofluidics*, vol. 7, no. 4, pp. 531–543, 2009.

[15] T. Metz, N. Paust, C. MÃijller, R. Zengerle, and P. Koltay, "Passive water removal in fuel cells by capillary droplet actuation," *Sensors and Actuators A: Physical*, vol. 143, no. 1, pp. 49 – 57, 2008. Micromechanics Section of Sensors and Actuators (SAMM), based on contributions revised from the

Technical Digest of the {IEEE} 20th International Conference on Micro Electro Mechanical Systems (MEMS 2007) {MEMS} 2007 {IEEE} 20th International Conference on Micro Electro Mechanical Systems.

[16] T. Metz, N. Paust, R. Zengerle, and P. Koltay, “Capillary driven movement of gas bubbles in tapered structures,” *Microfluidics and Nanofluidics*, vol. 9, no. 2-3, pp. 341–355, 2010.

[17] A. Gunther, S. A. Khan, M. Thalmann, F. Trachsel, and K. F. Jensen, “Transport and reaction in microscale segmented gas-liquid flow,” *Lab Chip*, vol. 4, no. 4, pp. 278–86, 2004. Gunther, Axel Khan, Saif A Thalmann, Martina Trachsel, Franz Jensen, Klavs F eng Research Support, Non-U.S. Gov't Research Support, U.S. Gov't, Non-P.H.S. England 2004/07/23 05:00 Lab Chip. 2004 Aug;4(4):278-86. Epub 2004 Jun 16.

[18] F. ÃŰzkan, K. Hecht, P. Pfeifer, K. Schubert, and B. Kraushaar-Czarnetzki, “Influence of the contact angle on two-phase flow in microreactors for nitrobenzeneâĂŞhydrogenâĂŞstainless steel/carbon,” *Surface and Interface Analysis*, vol. 42, no. 6-7, pp. 1122–1127, 2010.

[19] S. Slade, S. A. Campbell, T. R. Ralph, and F. C. Walsh, “Ionic conductivity of an extruded nafion 1100 ew series of membranes,” *Journal of The Electrochemical Society*, vol. 149, no. 12, pp. A1556–A1564, 2002.

[20] K. Kreuer, “On the development of proton conducting polymer membranes for hydrogen and methanol fuel cells,” *Journal of Membrane Science*, vol. 185, no. 1, pp. 29 – 39, 2001. Membrances in Fuel Cells.

[21] P. Choi, N. Jalani, and R. Datta, “Thermodynamics and proton transport in nafion ii. proton diffusion mechanisms and conductivity,” *Journal of the Electrochemical Society*, vol. 152, no. 3, pp. E123–E130, 2005.

[22] H. Chinen, K. Mawatari, Y. Pihosh, K. Morikawa, Y. Kazoe, T. Tsukahara, and T. Kitamori, “Enhancement of proton mobility in extended-nanospace channels,” *Angewandte Chemie International Edition*, vol. 51, no. 15, pp. 3573–3577, 2012.

[23] S. Moghaddam, E. Pengwang, Y.-B. Jiang, A. R. Garcia, D. J. Burnett, C. J. Brinker, R. I. Masel, and M. A. Shannon, “An inorganic-organic proton exchange membrane for fuel cells with a controlled nanoscale pore structure,” *Nat Nano*, vol. 5, pp. 230–236, Mar. 2010.

[24] R. M. Tiggelaar, V. Verdoold, H. Eghbali, G. Desmet, and J. G. E. Gardeniers, “Characterization of porous silicon integrated in liquid chromatography chips,” *Lab Chip*, vol. 9, pp. 456–463, 2009.

[25] M. Sailor, *Porous silicon in practice preparation, characterization and applications*. Weinheim: Wiley-VCH, 2012.

[26] S. Sukas, R. M. Tiggelaar, G. Desmet, and H. J. G. E. Gardeniers, “Fabrication of integrated porous glass for microfluidic applications,” *Lab Chip*, vol. 13, pp. 3061–3069, 2013.

[27] S. S. Mammana, A. Greatti, F. H. Luiz, F. I. da Costa, A. P. Mammana, G. A. Calligaris, L. P. Cardoso, C. I. Mammana, and D. den Engelsen, “Study of wet etching thin films of indium tin oxide in oxalic acid by monitoring the resistance,” *Thin Solid Films*, vol. 567, pp. 20 – 31, 2014.

[28] J. Tymoczko, F. Calle-Vallejo, W. Schuhmann, and A. S. Bandarenka, “Making the hydrogen evolution reaction in polymer electrolyte membrane electrolysers even faster,” *Nature Communications*, vol. 7, p. 10990, mar 2016.

Appendices

A. Production details

In this appendix, the details of producing the porous silicon membranes and channels are shown. This chapter is cited from the Master Thesis by Saskia Schildkamp, MSc, Mesoscale Systems, 2014.

Chapter 3

Fabrication of Chips with Porous Silicon Membranes

3.1 Experimental Set-up

A single-cell Teflon reservoir was used for the electrochemical etching of silicon wafers. The wafer was positioned inside the Teflon holder and sealed with a leak-tight O-ring. The backside (unpolished) of the wafer was in direct contact with a copper electrode (anode) of 3 mm thick which covered the entire backside. The front side (polished) was exposed to an electrolyte solution in the form of aqueous hydrogen fluoride (HF). A platinum counter electrode (cathode, a mesh of platinum (Pt) wire with a diameter 0.4mm) was immersed in this solution to complete the electrical circuit. The cathode was positioned on a Teflon separator ring, which was placed on the wafer, in order to maintain an uniform anodization process. In this way a 5 mm separation was realized between the platinum and the wafer. A Keithley (Model 2410) high voltage source meter was used for applying a potential to the anode while the cathode was grounded. Figure 3.1.1 shows a schematic representation of the experimental set-up.

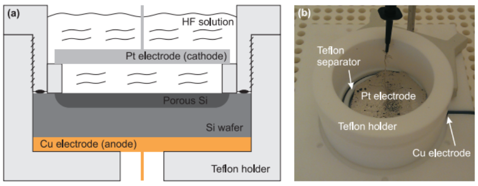

Figure 3.1.1: Schematic representation (a), and a picture (b) of the anodization chamber [19].

3.2 Chip Fabrication 'Vertical-oriented Pores'

The fabrication of chips containing porous areas in combination with flow channels in glass is given in this section. Figure 3.2.1 shows the process scheme. The fabrication of both wafers is separately

outlined in the following sections, the flow sheet can be found in Appendices B, C and D.

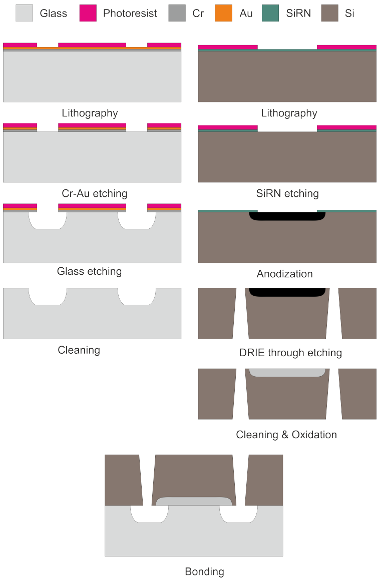

Figure 3.2.1: Process scheme; fluidic channels in glass wafer bonded to a silicon wafer with porous areas. Oxidation is optional. Cross-sectional view.

3.2.1 Fabrication of the Fluidic Channels in a Glass Wafer

Prior to processing the glass substrates (MEMPax, 100 mm diameter, 500 µm thick, w/o flats, Schott) were cleaned via immersion in fuming (99%) HNO_3 (2x 5 min) followed by DI-water rinsing and drying. A gold/chromium (Au/Cr) layer was sputtered on one side of the wafer. Cr was sputtered first for 1 min as an adhesion layer (deposition rate: 15 nm/min) followed by the Au for 2.5 minutes (deposition rate: 45 nm/min) under an argon atmosphere. Afterwards photoresist was applied (Olin 907-17) and standard UV-lithography was performed to define the fluidic channels. This was followed by ozone treatment of the OiR resist to improve wetting of the Au/Cr layer. Thereafter, the Au and Cr layers were etched with standard etchants. A Veeco-Dektak profilometry measurement was done to measure the thickness of the Olin layer and Au/Cr film prior to the glass etching. Dicing foil is applied on the backside of the wafer prior to the etching in HF for protection purposes. 25 % HF is used for the etching of the flow channels with a depth between 50 and 75 µm (etch rate: 1 µm/min). Afterwards the photoresist is stripped via immersion in HNO_3(99%) and the remaining Au/Cr mask is stripped via the same wet etching procedure as done for the channels, followed by quick dump rinsing and drying. The final width and depth of the structures in glass is measured with a Veeco-Dektak profilometer. Prior to the anodic bonding the wafer was exposed to another standard cleaning step; 2x 5 minutes immersion in 99% HNO_3 followed by a quick dump rinsing cycle and drying.

3.2.2 Fabrication of Porous Areas in a Silicon Wafer

The porous areas and fluidic accesses are fabricated in heavily boron doped silicon wafers (p^{++} Si, 100 mm diameter, resistivity 0.010-0.025 Ωcm, <100> -oriented, 525 µm thick, single side polished; Okmetic, Finland). It is started with a standard cleaning process; 2x 5 minutes immersion in fuming 99% nitric acid (HNO_3), followed by 15 minutes in boiling HNO_3 (69%) and quick dump rinsing in de-mineralized (DI) water. Afterwards a 1% hydrofluoric acid (HF) dip (1 min) is done to remove native oxide prior to the silicon nitride deposition, followed by another cycle of quick dump rinsing and spin drying. Low pressure chemical vapor deposition (LPCVD) was used for the deposition of a 250 nm thick low stress silicon-rich silicon nitride layer (SiRN). By means of standard UV-lithography the porous areas were defined on the topside of the wafers in photoresist (Olin 907-17). The photoresist pattern was transferred into the SiRN layer via reactive ion etching for ca. 4 minutes (RIE; Tetske, etchrate 60 nm/min). This was followed by stripping of the resist in oxygen plasma and cleaning of the substrate in Piranha ($H_2SO_4 : H_2O_2 (3:1)$ vol% for 15 min.).

The anodization is performed in a 5% HF solution for 2 minutes under a constant potential mode with an applied voltage of 200 mV. Stripping of the SiRN layer can only be done immediately after anodization in a 50% HF solution for 100 minutes. Cleaning afterward has to be done with Piranha cleaning (15 min) and a cascade rinsing with DI water followed by ethanol immersion and drying by evaporation to prevent the porous structure from damaging. Thermal oxidation can be performed in order to enhance the hydrophilicity of the structure. UV-lithography on the bottom side of the wafer is done to define the fluidic access holes in photoresist (Olin 908-35). With deep reactive ion etching (DRIE, B-Uniform recipe; Adixen AMS100SE) the access holes are created. Oxygen plasma treatment and Piranha cleaning are required to strip the remaining photoresist. Bonding with the MEMPax wafer with fluidic channels was done via anodic bonding. Afterwards the chips are diced (Disco DAD 321) where the fluidic accesses are covered with UV-curable dicing foil and faced downwards during dicing.

3.3 Chip Fabrication 'Horizontal-oriented pores'

The second design has fluidic channels etched in the silicon which are separated by a porous membrane. The patterned silicon wafer is bonded to a flat glass wafer. A schematic process scheme can be seen in Figure 3.3.1.

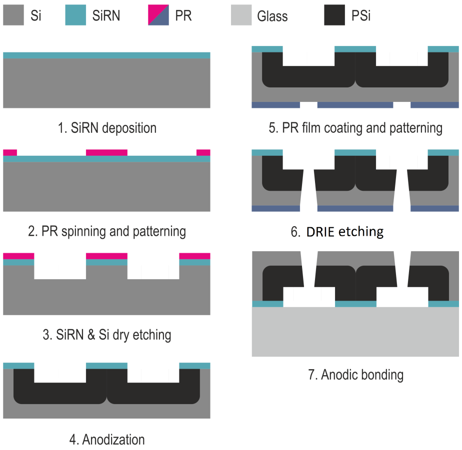

Figure 3.3.1: Process scheme; etched silicon substrate used to obtain a porous wall between two fluidic channels. Cross-sectional view.

3.3.1 Fabrication of Porous Membranes

The type of wafers used are heavily boron doped silicon wafers (p^{++} Si, 100 mm diameter, resistivity 0.010-0.025 Ωcm, <100> -oriented, 525 µm thick, single side polished; Okmetic, Finland). The wafers were treated with a standard cleaning; immersion in fuming 100% nitric acid (HNO_3) (2x 5 min), boiling 69% nitric acid (15 min) and quick dump rinsing in DI water. This cleaning process was followed by a 1% HF dip (1 min) to remove native oxide prior to the silicon nitride deposition and another cycle of quick dump rinsing. The wafers were dried via spin drying. A layer of 250 nm silicon-rich silicon nitride (SiRN) was deposited on the wafers using low pressure chemical vapor deposition (LPCVD). Photoresist (Olin 907-17) was applied to the topside and standard UV-lithography was used to define the fluidic network in this photoresist (Olin 907-17). The photoresist pattern was transferred into the SiRN layer via reactive ion etching of the SiRN layer (RIE; Adixen AMS100DE; $C_4F_8 + He + CH_4$, 1 min etch time). This was followed by deep reaction ion etching (DRIE; Adixen AMS100SE) of silicon with the Bosch process (B-HARS recipe). The etching time was 3 minutes, which resulted in 10 µm deep channels. The SiRN layer of the bottom side was removed via the previous RIE technique. Standard UV-Lithography on the bottom side of the wafer was done with

Olin 908-35 photoresist to define the fluidic accesses. These access holes were etched into the silicon to a depth of 380-400 µm with DRIE (B-Uniform recipe; Adixen AMS100SE). Post to the etching the photoresist layers were stripped from top- and backside with an oxygen plasma. Piranha cleaning ($H_2SO_4 : H_2O_2 (3:1)$ vol% for 15 min.) was performed afterwards in order to remove any remaining fluorocarbons, followed by DI water rinsing and drying.

The anodization is performed in the single Teflon reservoir set-up, which is described in Section 3.1. A constant-current mode is used and according to the silicon area exposed to the electrolyte a current of 25 mA was used in order to avoid electropolishing. An electrolyte concentration of 5% HF was used. Ethanol (EtOH) can be added to the electrolyte to avoid sticking of generated hydrogen to the surface, in a volumetric ratio of 5 : 1 HF : ethanol. Hydrogen bubbles can create locally isolated regions which prevent pore formation to occur and will negatively influence the uniformity of the porous layer. It was experimentally found that an anodization time of 30 minutes was optimal to obtain a fully porous-Si membrane. SiRN stripping after the anodization is not required for this design. Immediately after the defined anodization time the electrolyte solution was removed and the substrate was cascade rinsed with DI water. After this the wafer was immersed in ethanol (>1h) and dried in the wet bench by means of evaporation. Piranha cleaning (15 min) was performed afterward in order to remove possible traces of the Cu anode from the backside of the wafers, followed by again cascade rinsing, ethanol immersion (>1h) and drying by means of evaporation in the wet bench (>2h).

Blank MEMPax (100 mm diameter, 500 µm thick, w/o flats, Schott) glass wafers were used for anodic bonding to enclose the fluidic network. Afterwards the access holes to the fluidic network were opened by DRIE (B-Uniform recipe; Adixen AMS100SE). A Disco DAD 321 dicing system was used to dice the chips, during which the fluidic accesses were covered with UV-curable dicing foil and faced downwards.

B. Matlab Scripts

In this appendix, the Matlab code used to generate the structures as shown in Chapter 5: Integrating & Combining is reproduced. The first M-file is used to set the parameters and run the main loop; the second M-file is a function to generate the necessary coordinates for drawing the structures. The third M-file is an alternative for the first; creating a tapered serpentine similar to the first but with a more continuous taper and membrane width. Images are provided to show an example of the final results of these scripts in Clewin.

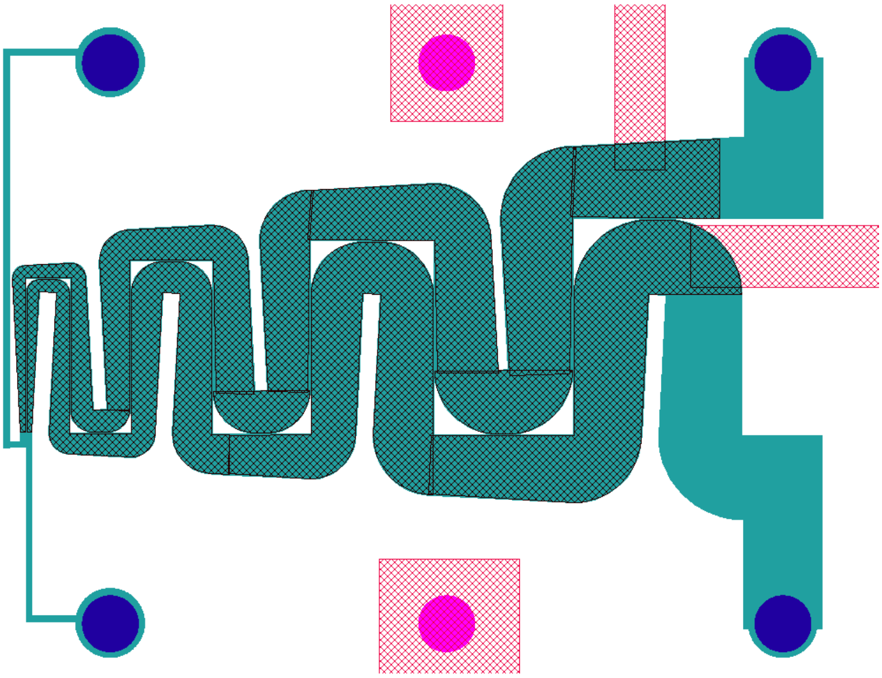

Figure B.1: Clewin screenshot of the primary method of producing tapered channels using the Matlab script below. This design is more rough around the edges compared to the alternative design, including a messier code, but is easier to understand/read and produce because of larger allowable tolerances in the design. This was the design that was eventually used for experiments.

```
% taperedchannels.m
% Matlab code to produce two parallel tapered channels in Clewin that serpentine.
% Run this code directly in Clewin by using the "Insert Script" function.
% Needs the matlab toolbox provided by Clewin found at...
% ...http://www.wieweb.com/download/mltoolbox.zip
% Needs the function clewinfilledChannel.m to work properly.
```

```
% Made by Samuel Mok for Mesoscale Chemical Systems, University Twente, 2015
% Contact: samopsa@gmail.com
%Initial Parameters
xstart=0;                           %starting x-coordinate
ystart=0;                           %starting y-coordinate
turns=7;                            %number of windings the structure needs
membrane=10;                        %membrane thickness, i.e. distance between...
                                    %...channel 1 and 2
endWidth=1000;                      %length of last channel -- to ensure tapered...
                                    %... channel that moves to the fluid outlet
lengthstart=2500;                   %length of channel for each winding
widthstart=100;                     %starting width of channel
angle=3*0.0174532925;               %angle converted to radians from degrees
widthtaper=lengthstart*tan(angle);  %tapering width increase -- calculate from angle
distancestart=300;                  %distance between turns of a single channel
orientationstart='bottomtopL';      %start at the bottom, moves to the top. Currently..
                                    %...the only supported version.
Sideorientation='leftrightT';       %this script currently only supports...
                                    %...left-to-right serpentines
%initialize first set of channels by copying parameters
lengthtaper=lengthstart;
orientation=orientationstart;
lengthtaperstart=lengthtaper;
widthtaperstart=widthtaper;
width=widthstart;
length=lengthstart;
x=xstart;
y=ystart;
distance=distancestart;
area=0 %set area to zero, used to additively store the area of the tapered serpentine

%Main program loop to draw the first channel, runs for <turns> amount of times
%Each loop draws a channel up, right, down and right again to create a winding
for i=1:turns+1
    %draw the first channel: straight
    %calculate the width of tapering from the angle
    widthtaper=length*tan(angle)
    %get all the nodes (ie polygon coordinates) for drawing the first channel
    nodesvert{i}=clewinfilledChannel(x,y,width,length,widthtaper,orientation)
    polygon(nodesvert{i})   %draw the polygon
    %add to total area
    area=area+polyarea(nodesvert{i}(:,1),nodesvert{i}(:,2))
    %get coordinates to start from the end points of the previous channel
    %depends on going up or down
    if strcmp(orientation,'bottomtopL')
        Sidex=nodesvert{i}(4,1)
        Sidey=nodesvert{i}(4,2)
    elseif strcmp(orientation,'topbottomR')
        Sidex=nodesvert{i}(3,1)
        Sidey=nodesvert{i}(3,2)-width-widthtaper
    end
    Sidewidth=width+widthtaper %increase the width by the increase in tapering
    %calculate length of turn, depends on width of the channel and the tapering
    if i~=turns+1 %nod needed for the last part
        if mod(i,2)==0      %even
            Sidelength=(width+widthtaper)*2+distance+(distance*tan(angle))+2*membrane
        else                %uneven
            Sidelength=distance
        end
```

```
    else
    Sidelength=endWidth
    end
    %calculate taperwidth and draw, similar to straight channel
    Sidewidthtaper=Sidelength*tan(angle)
    nodeshor{i}=clewinfilledChannel(Sidex,Sidey,Sidewidth,Sidelength...
    ,Sidewidthtaper,Sideorientation)
    if i~=turns+1
    area=area+polyarea(nodeshor{i}(:,1),nodeshor{i}(:,2))
    end
    polygon(nodeshor{i})

    if strcmp(orientation,'bottomtopL')
        %smooth channels
        %Method: Draw circle with corner as middle and width as radius
        %then cut off 3/4 of the circle to leave only necessary part
        %this will create a quarter circle as the connecting part between vertical...
        %...and horizontal channels
        circle1=cleConvert(cleCircle(Sidex,Sidey,Sidewidth));
        x(1)=Sidex;
        y(1)=Sidey;
        x(2)=x(1);
        y(2)=y(1)+Sidewidth;
        x(3)=x(2)+Sidewidth;
        y(3)=y(2);
        x(4)=x(3);
        y(4)=y(3)-2*Sidewidth;
        x(5)=x(4)-2*Sidewidth;
        y(5)=y(4);
        x(6)=x(5);
        y(6)=y(5)+Sidewidth;
        cutoffnodes1=[x;y]';
        cutoff1=cleConvert(clePolygon(cutoffnodes1));
        cleDraw(cleSubstract(circle1,cutoff1))
        area=area+0.25*pi*Sidewidth^2
        %second corner circle
        if i~=turns+1
        circle3=cleConvert(cleCircle(Sidex+Sidelength,Sidey-Sidewidthtaper,...
        Sidewidth+Sidewidthtaper));
        x(1)=Sidex+Sidelength;
        y(1)=Sidey-Sidewidthtaper;
        x(2)=x(1);
        y(2)=y(1)+Sidewidth+Sidewidthtaper;
        x(3)=x(2)-Sidewidth-Sidewidthtaper;
        y(3)=y(2);
        x(4)=x(3);
        y(4)=y(3)-2*(Sidewidth+Sidewidthtaper);
        x(5)=x(4)+2*(Sidewidth+Sidewidthtaper);
        y(5)=y(4);
        x(6)=x(5);
        y(6)=y(5)+Sidewidth+Sidewidthtaper;
        cutoffnodes3=[x;y]';
        cutoff3=cleConvert(clePolygon(cutoffnodes3));
        cleDraw(cleSubstract(circle3,cutoff3))
        area=area+0.25*pi*(Sidewidth+Sidewidthtaper)^2
        end
        %settings for next loop
        orientation='topbottomR'
        x=nodeshor{i}(4,1)
```

```
        y=nodeshor{i}(4,2)
    elseif strcmp(orientation,'topbottomR')
        %smooth corners, same as above but with different coordinates
        %first corner circle 1
        circle1=cleConvert(cleCircle(Sidex,Sidey+Sidewidth,Sidewidth));
        x(1)=Sidex;
        y(1)=Sidey+Sidewidth;
        x(2)=x(1);
        y(2)=y(1)-Sidewidth;
        x(3)=x(2)+Sidewidth;
        y(3)=y(2);
        x(4)=x(3);
        y(4)=y(3)+2*Sidewidth;
        x(5)=x(4)-2*Sidewidth;
        y(5)=y(4);
        x(6)=x(5)
        y(6)=y(5)-Sidewidth;
        cutoffnodes1=[x;y]';
        cutoff1=cleConvert(clePolygon(cutoffnodes1));
        cleDraw(cleSubstract(circle1,cutoff1))
        area=area+0.25*pi*(Sidewidth)^2
        %second corner circle 1
        if i~=turns+1
        circle3=cleConvert(cleCircle(Sidex+Sidelength,Sidey+Sidewidth,...
        Sidewidth+Sidewidthtaper));
        x(1)=Sidex+Sidelength;
        y(1)=Sidey+Sidewidth;
        x(2)=x(1);
        y(2)=y(1)-Sidewidth-Sidewidthtaper;
        x(3)=x(2)-Sidewidth-Sidewidthtaper;
        y(3)=y(2);
        x(4)=x(3);
        y(4)=y(3)+2*(Sidewidth+Sidewidthtaper)
        x(5)=x(4)+2*(Sidewidth+Sidewidthtaper);
        y(5)=y(4);
        x(6)=x(5)
        y(6)=y(5)-Sidewidth-Sidewidthtaper;
        cutoffnodes3=[x;y]';
        cutoff3=cleConvert(clePolygon(cutoffnodes3));
        cleDraw(cleSubstract(circle3,cutoff3))
        area=area+0.25*pi*(Sidewidth+Sidewidthtaper)^2
        end
        %settings for next loop
        orientation='bottomtopL'
        x=nodeshor{i}(3,1)
        y=nodeshor{i}(3,2)
    end
    width=width+widthtaper+Sidewidthtaper
end

%Main program loop to create the second channel parallel to the first
%Reset parameters to initial values
%See beginning for details
lengthtaper=lengthstart;
widthtaper=lengthstart*tan(angle);
orientationstart='bottomtopR';
Sideorientation='leftrightB'
orientation=orientationstart;
lengthtaperstart=lengthtaper;
```

```
widthtaperstart=widthtaper;
width=widthstart;
length=lengthstart;
x=xstart;
y=ystart;
distance=distancestart;
%start the loop, same as before but everything is shifted to the right or down
for i=1:turns
    if strcmp(orientation,'bottomtopR')
        if i==1
            y=nodesvert{i}(2,2)
            x=nodesvert{i}(2,1)-membrane-width
        else
            y=nodeshor2{i-1}(4,2)
        end
        length=nodeshor{i}(2,2)+membrane-y
    else
        x=nodesvert{i}(2,1)+membrane
        y=nodeshor{i-1}(3,2)+membrane
        length=y-nodeshor{i}(2,2)-membrane-width-(124-i*0.5)
    end
    widthtaper=length*tan(angle)
    debug(i)=widthtaper
    nodesvert2{i}=clewinfilledChannel(x,y,width,length,widthtaper,...
    orientation)
    polygon(nodesvert2{i})
    area=area+polyarea(nodesvert2{i}(:,1),nodesvert2{i}(:,2))
    if strcmp(orientation,'bottomtopR')
        Sidex=nodesvert2{i}(3,1)
        Sidey=nodesvert2{i}(3,2)
    elseif strcmp(orientation,'topbottomL')
        Sidex=nodesvert2{i}(4,1)
        Sidey=nodesvert2{i}(4,2)-width-widthtaper
    end
    Sidewidth=width+widthtaper
    if mod(i,2)==1
    %uneven
        if i~=turns
        Sidelength=nodesvert{i+1}(2,1)-Sidex+membrane
        else
        Sidelength=nodeshor{i}(3,1)-Sidex+widthtaper+Sidewidth+endWidth
        end
    else
    %even
        Sidelength=(nodesvert{i+1}(2,1)-Sidex-width-widthtaper-membrane)...
        /(tan(angle)+1)
    end
    Sidewidthtaper=Sidelength*tan(angle)
    nodeshor2{i}=clewinfilledChannel(Sidex,Sidey,Sidewidth,Sidelength,...
    Sidewidthtaper,Sideorientation)
    polygon(nodeshor2{i})
    if i~=turns
    area=area+polyarea(nodeshor2{i}(:,1),nodeshor2{i}(:,2))
    end
    if strcmp(orientation,'bottomtopR')
    %smooth channels
        %first corner circle
        circle1=cleConvert(cleCircle(Sidex,Sidey,Sidewidth));
        x(1)=Sidex;
```

```
        y(1)=Sidey;
        x(2)=x(1);
        y(2)=y(1)+Sidewidth;
        x(3)=x(2)+Sidewidth;
        y(3)=y(2);
        x(4)=x(3);
        y(4)=y(3)-2*Sidewidth;
        x(5)=x(4)-2*Sidewidth;
        y(5)=y(4);
        x(6)=x(5)
        y(6)=y(5)+Sidewidth;
        cutoffnodes1=[x;y]';
        cutoff1=cleConvert(clePolygon(cutoffnodes1));
        cleDraw(cleSubstract(circle1,cutoff1))
        area=area+0.25*pi*(Sidewidth)^2
        %second corner circle
        if i~=turns
        circle3=cleConvert(cleCircle(Sidex+Sidelength,Sidey,...
        Sidewidth+Sidewidthtaper));
        x(1)=Sidex+Sidelength;
        y(1)=Sidey;
        x(2)=x(1);
        y(2)=y(1)+Sidewidth+Sidewidthtaper;
        x(3)=x(2)-Sidewidth-Sidewidthtaper;
        y(3)=y(2);
        x(4)=x(3);
        y(4)=y(3)-2*(Sidewidth+Sidewidthtaper);
        x(5)=x(4)+2*(Sidewidth+Sidewidthtaper);
        y(5)=y(4);
        x(6)=x(5);
        y(6)=y(5)+Sidewidth+Sidewidthtaper;
        cutoffnodes3=[x;y]';
        cutoff3=cleConvert(clePolygon(cutoffnodes3));
        cleDraw(cleSubstract(circle3,cutoff3))
        area=area+0.25*pi*(Sidewidth+Sidewidthtaper)^2
        end
        orientation='topbottomL'
        x=nodeshor2{i}(4,1)
        y=nodeshor2{i}(4,2)
    elseif strcmp(orientation,'topbottomL')
        circle1=cleConvert(cleCircle(Sidex,Sidey+Sidewidth,Sidewidth));
        x(1)=Sidex;
        y(1)=Sidey+Sidewidth;
        x(2)=x(1);
        y(2)=y(1)-Sidewidth;
        x(3)=x(2)+Sidewidth;
        y(3)=y(2);
        x(4)=x(3);
        y(4)=y(3)+2*Sidewidth;
        x(5)=x(4)-2*Sidewidth;
        y(5)=y(4);
        x(6)=x(5)
        y(6)=y(5)-Sidewidth;
        cutoffnodes1=[x;y]';
        cutoff1=cleConvert(clePolygon(cutoffnodes1));
        cleDraw(cleSubstract(circle1,cutoff1))
        area=area+0.25*pi*(Sidewidth)^2
        %second corner circle 1
        if i~=turns
```

```
        circle3=cleConvert(cleCircle(Sidex+Sidelength,...
        Sidey+Sidewidth+Sidewidthtaper,Sidewidth+Sidewidthtaper));
        x(1)=Sidex+Sidelength;
        y(1)=Sidey+Sidewidth+Sidewidthtaper;
        x(2)=x(1);
        y(2)=y(1)-Sidewidth-Sidewidthtaper;
        x(3)=x(2)-Sidewidth-Sidewidthtaper;
        y(3)=y(2);
        x(4)=x(3);
        y(4)=y(3)+2*(Sidewidth+Sidewidthtaper);
        x(5)=x(4)+2*(Sidewidth+Sidewidthtaper);
        y(5)=y(4);
        x(6)=x(5);
        y(6)=y(5)-Sidewidth-Sidewidthtaper;
        area=area+0.25*pi*(Sidewidth+Sidewidthtaper)^2
        cutoffnodes3=[x;y]';
        cutoff3=cleConvert(clePolygon(cutoffnodes3));
        cleDraw(cleSubstract(circle3,cutoff3))
        end
        orientation='bottomtopR'
        x=nodeshor2{i}(3,1)
        y=nodeshor2{i}(3,2)
    end
    width=width+widthtaper+Sidewidthtaper
end
```

```
%clewinfilledChannel.m
function [nodes]=clewinfilledChannel(xstart,ystart,width,length,taperwidth,orientation)
%Makes an array that contains the coordinates needed to make...
%...a tapered channel polygon in clewin
%Made by Samuel Mok for Mesoscale Chemical Systems, University Twente, 2015
%Contact: samopsa@gmail.com
%parameters:
%xstart,ystart is starting coordinates
%length is channel length
%width is channel width
%taperwidth is added width of taper

if strcmp(orientation,'bottomtopL')
    x(1)=xstart+width;
    y(1)=ystart;

    x(2)=xstart;
    y(2)=ystart;

    x(3)=xstart;
    y(3)=ystart+length;

    x(4)=x(1)+taperwidth;
    y(4)=ystart+length;

    nodes=[x;y]';

elseif strcmp(orientation,'bottomtopR')
    x(1)=xstart;
    y(1)=ystart;

    x(2)=xstart+width;
    y(2)=ystart;

    x(3)=xstart+width;
    y(3)=ystart+length;

    x(4)=xstart-taperwidth;
    y(4)=ystart+length;

    nodes=[x;y]';
elseif strcmp(orientation,'topbottomL')
    x(1)=xstart+width;
    y(1)=ystart;

    x(2)=xstart;
    y(2)=ystart;

    x(3)=xstart;
    y(3)=ystart-length;

    x(4)=xstart+width+taperwidth;
    y(4)=ystart-length;

    nodes=[x;y]';
elseif strcmp(orientation,'topbottomR')
    x(1)=xstart;
    y(1)=ystart;
```

```
    x(2)=xstart+width;
    y(2)=ystart;

    x(3)=xstart+width;
    y(3)=ystart-length;

    x(4)=xstart-taperwidth;
    y(4)=ystart-length;

    nodes=[x;y]';
elseif strcmp(orientation,'leftrightT')

    x(1)=xstart;
    y(1)=ystart;

    x(2)=xstart;
    y(2)=y(1)+width

    x(3)=xstart+length;
    y(3)=y(1)+width;

    x(4)=xstart+length;
    y(4)=y(1)-taperwidth;

    nodes=[x;y]';

elseif strcmp(orientation,'leftrightB')

    x(1)=xstart;
    y(1)=ystart+width;

    x(2)=xstart;
    y(2)=ystart;

    x(3)=xstart+length;
    y(3)=ystart;

    x(4)=xstart+length;
    y(4)=y(1)+taperwidth;

    nodes=[x;y]';
    %possibe orientations: 'topbottom', 'bottomtop', 'rightleft', 'leftright'
elseif strcmp(orientation,'leftright')

    x(1)=xstart;
    y(1)=ystart;

    x(2)=xstart;
    y(2)=ystart+width;

    x(3)=xstart+length;
    y(3)=ystart+width;

    x(4)=xstart+length;
    y(4)=ystart;

    nodes=[x;y]';
```

```
elseif strcmp(orientation,'rightleft')

    x(1)=xstart;
    y(1)=ystart;

    x(2)=xstart;
    y(2)=ystart-width;

    x(3)=xstart-length;
    y(3)=ystart-width;

    x(4)=xstart-length;
    y(4)=ystart;

    nodes=[x;y]';

elseif strcmp(orientation,'topbottom')
    x(1)=xstart;
    y(1)=ystart;

    x(2)=xstart+width;
    y(2)=ystart;

    x(3)=xstart+width;
    y(3)=ystart-length;

    x(4)=xstart;
    y(4)=ystart-length;

    nodes=[x;y]';
elseif strcmp(orientation,'bottomtop')
    x(1)=xstart;
    y(1)=ystart;

    x(2)=xstart-width;
    y(2)=ystart;

    x(3)=xstart-width;
    y(3)=ystart+length;

    x(4)=xstart;
    y(4)=ystart+length;

    nodes=[x;y]';
end
```

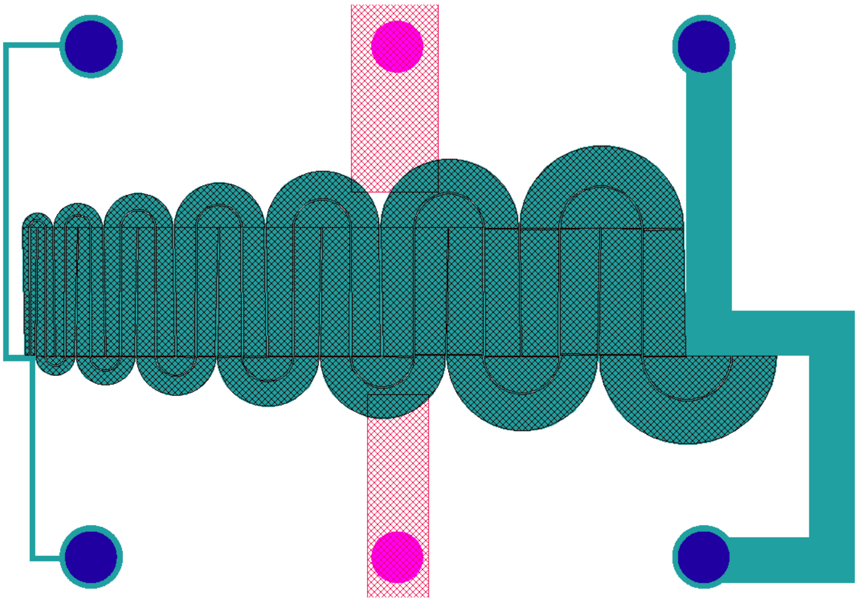

Figure B.2: Clewin screenshot of the alternative method of producing tapered channels using the Matlab script below. As can be seen, this design method is a lot more smooth and regular, and the code is more compact. However, during production the small allowable tolerances caused issues. This lead to no chip of this design being successfully produced, and thus it was not experimentally tested.

```
% taperedchannelsalternative.m
% Matlab code to produce two parallel tapered channels in Clewin that serpentine.
% This alternative method is more compact and features a more continuous taper.
% However the code is less 'readable' and the design is more cramped.
% Run this code directly in Clewin by using the "Insert Script" function.
% Needs the matlab toolbox provided by Clewin found at...
% ...http://www.wieweb.com/download/mltoolbox.zip
% Made by Pieter Westerik and Samuel Mok for...
% ... Mesoscale Chemical Systems, University Twente, 2015
% Contact: samopsa@gmail.com
%Initial Parameters

dwdx=0.016; %width increase per channel length
ws=100;     %starting width
d=10;       %membrane width
lw=2500;    %winding length
nw=7;       %number of windings
x=0;        %starting x-coordinate

width=ws;
phi=linspace(0,pi,20)';

for iw=1:nw;
clePolygon([[x-d/2 0]; [x-d/2 lw]; [x-d/2-width-lw*dwdx lw]; [x-d/2-width 0]]);
clePolygon([[x+d/2 0]; [x+d/2 lw]; [x+d/2+width+lw*dwdx lw]; [x+d/2+width 0]]);
width=width+lw*dwdx;
wend=(width*(1+dwdx)+2*d*dwdx)/(1-dwdx);
clePolygon([[x+d+width-d/2.*cos(phi) lw+d/2.*sin(phi)];...
 [x+d/2+(d+width+wend)/2.*(1+cos(phi)) lw+(d+width+wend)/2.*sin(phi)]]);
```

```
clePolygon([[x+d+wend-(width+wend+3/2*d).*cos(phi)...
 lw+(width+wend+3/2*d).*sin(phi)]; [x-d/2+(3*d+width+wend)...
 /2.*(1+cos(phi)) lw+(3*d+width+wend)/2.*sin(phi)]]);
x=x+2*d+width+wend;
width=wend;
clePolygon([[x-d/2 lw]; [x-d/2 0]; [x-d/2-width-lw*dwdx 0];...
 [x-d/2-width lw]]);
clePolygon([[x+d/2 lw]; [x+d/2 0]; [x+d/2+width+lw*dwdx 0];...
 [x+d/2+width lw]]);
width=width+lw*dwdx;
wend=(width*(1+dwdx)+2*d*dwdx)/(1-dwdx);
clePolygon([[x+d+width-d/2.*cos(phi) -d/2.*sin(phi)];...
 [x+d/2+(d+width+wend)/2.*(1+cos(phi)) -(d+width+wend)/2.*sin(phi)]]);
clePolygon([[x+d+wend-(width+wend+3/2*d).*cos(phi)...
 -(width+wend+3/2*d).*sin(phi)]; [x-d/2+(3*d+width+wend)/2.*(1+cos(phi))...
 -(3*d+width+wend)/2.*sin(phi)]]);
x=x+2*d+width+wend;
width=wend;
end;
```

C. Porous silicon membrane experiments

In this appendix, 2 reports are shown that were made by students under the supervision & assistance of the author of this thesis. The students investigated the resistance of the porous silicon membrane by performing electrical measurements. Their main conclusions were that the current setup is not usable for quantitative experiments.

6/30/2015

Study on the influence of salts on the resistance of porous silicon membrane

Project Materials and Molecular Science and Technology

Ronald Jong & Mariël Elshof
Supervisors: Sebastiaan Wisman, Samuel Mok,
David Fernandez Rivas

UNIVERSITY OF TWENTE

Table of Contents

---

1. Introduction

The energy consumption of the world is growing. However, the main resources for the production of energy are not renewable and therefore research is done on renewable energy sources. One of the possible renewable energy sources is hydrogen gas [1].

This project is based on the overall idea to produce hydrogen fuel from water by its dissociation as shown in reaction (1) due to solar irradiation in for example microfluidic devices.

$$H_2O \rightarrow \frac{1}{2}O_2 + H_2 \qquad (1)$$

Water is split into oxygen gas, protons and electrons by a photocatalytic oxidation reaction. At the cathode hydrogen gas is formed from the protons and electrons produced in the dissociation reaction of water. The oxidation and reduction half-reactions are given in reactions (2) and (3).

$$H_2O \rightarrow \frac{1}{2}O_2 + 2H^+ + 2e^- \qquad (2)$$

$$2H^+ + 2e^- \rightarrow H_2 \qquad (3)$$

Both electrons and protons need to be transferred between the photocatalysts. Electrons are transferred though electrical conduction by a metallic connection [2]. Protons could be transferred through the solution however a separated production of the gases is desired, as mixture of oxygen and hydrogen gas is extremely explosive and hard to separate [3]. To this end a proton conducting membrane is applied between the two channels in order to transportthe protons but not allow for any other material transport. The protons are transferred through the proton conducting membrane into the other channel.

In the last few years research is done on Nafion as a proton conducting membrane. However, because it swells it is not practical to use in microfluidic devices. Porous silicon has gained attention as a promising material to replace Nafion in the micro fuel generator [4]. Therefore research on the influence of several parameters on the transport in the porous silicon membrane is needed.

In this project a microfluidic chip which contains a nanoporous silicon membrane is studied. The contribution of the membrane to the total electrical resistance is characterized and the effect of several water based electrolytes is examined.

---

2. Theory

2.1. Nanoporous silicon membrane conductivity

The conductivity of H^+ and OH^- ions is significantly higher than that of other ions in water as a result of their movement through water by the formation and breaking of hydrogen bonds [5]. When ions are present in water, the water molecules will orient around the ion and form a so called hydration shell. Protons, on the other hand, will form a covalent bond with a water molecule to form a hydronium cation (H_3O^+). As a consequence protons are always inherently part of the water network. Hence, protons have unique mobility properties as they can move from their cation towards a neighboring water molecule to form a new cation. This phenomenon is called proton hopping and is described via the Grotthuss mechanism. The process repeats itself rapidly between hydronium and neighboring water molecules, which causes a flow of protonic character through the H_2O bulk. [4]

Porous silicon consists of a series of parallel nanochannels. Chinen et al. did research to the use of nanochannels instead of Nafion and showed that the proton diffusion coefficient in porous silicon has been shown to depend on pore equivalent diameter of the nanochannel (Figure 1) [6]. The graph shows a increase in diffusion coefficient by decreasing the pore diameter from to 180 nm. This is due to the increase in proton hopping. The small pore diameter cause a lower molecular motion of H_2O and results in an alignment of the H_2O molecules within the pores. At the surface of the porous silicon, a native layer of silicon oxide exists. Subjected to water, the silicon oxide gets hydrated and silicon hydroxyl (Si-OH) is formed at the surface. The Si-OH is able to transfer protons by the Grotthuss mechanism, thus protons are exchanged through the pores via the silica surface and H_2O molecules. [7] If it is assumed that the trend of increasing proton diffusion coefficient with lower pore diameter continues, this means that working with diameters in the low nano-range would have a benefit on the proton diffusion (porous silicon can have diameters in the range from 2 to 50 nm).The silicon hydroxyl groups may also play a role in the transfer of other ionic species. If this is indeed the case assisted transport should depend on the ion size and charge.

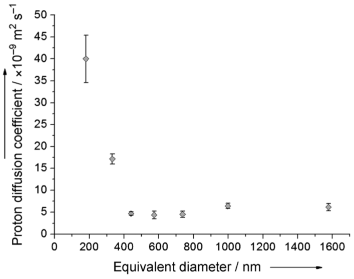

Figure 1. Proton diffusion coefficients for nanochannel sizes in the range of 180-1580 nm [6]

2.2. Electrolyte conductivity

An electrical current results from the motion of electrically charged particles in response to forces that act on them from an applied electric field. In water and ionic materials or fluids, a net motion of charged ions can occur. Because the electrical current is transported by the ions in solution, the conductivity, increases as the concentration of ions, the charge carriers in the solution, increases.

The Ohmic resistance of a simple two electrode electrochemical cell is defined by the ionic conductivity of the electrolyte, the distance between the electrodes and the electrode total surface area (A). When assuming an equal electrode surface for both electrodes the following definition of resistance is given:

$$R = \frac{L}{\kappa A} \tag{1}$$

In this equation R represents the resistance (Ω), L the distance between electrodes (m), A the electrode total surface area (m^2) and κ the specific conductivity of the electrolyte ($\Omega^{-1}\,m^{-1}$).

This specific conductivity is proportional to the electrolyte concentration, c ($mol\,m^{-3}$) and is related by the molar conductivity of the electrolyte, Λ ($\Omega^{-1}\,m^2\,mol^{-1}$):

$$\kappa = \Lambda c \tag{2}$$

The molar conductivity is defined as the conductivity of a 1 molar solution. For an infinite dilute solution the molar conductivity can be described as the sum of the individual ionic conductivities of the species present. Assuming an electrolyte of composed of a two ion salt solution the following relation is used:

$$\Lambda_0 = v_+\lambda_+^0 + v_-\lambda_-^0 \tag{3}$$

In this equation $v_\pm$ are the stoichiometric coefficients of the ions in the salt, λ is the individual ionic conductivity ($\Omega^{-1}\,m^2\,mol^{-1}$). The individual molar ionic conductivities for several ions are presented in In this equation, F is the Faraday constant (C mol^{-1}) and ΔV is the potential difference between working and reference electrode in (V).

Table 1. The ionic conductivity is a function of the ions size and its charge, increasing size and charge increases the ionic conductivity as shown for the cations. The total current that results from the ionic conductivity can thus be described by the following relation: [5]

$$I = \frac{F\left(\sum_j v_j \lambda_j^0 c_j\right)\Delta V}{L} \tag{4}$$

In this equation, F is the Faraday constant (C mol^{-1}) and ΔV is the potential difference between working and reference electrode in (V).

Table 1. Ion conduction for several common ions at 298 K. [5]

Cation	λ ($\Omega^{-1}\,m^2\,mol^{-1}$)	**Anion**	λ ($\Omega^{-1}\,m^2\,mol^{-1}$)
H^+	3.50	OH^-	1.98
Na^+	0.50	Cl^-	0.76
K^+	0.74	${NO_3}^-$	0.71
Ca^{2+}	1.20	${SO_4}^{2-}$	1.60

2.3. Application to the microfluidic system: expectations

For a simple electrochemical cell without a nanoporous silicon membrane the resistance of the system is expected to decrease in proportion with an increase in electrolyte conductivity. This theoretical trend is given by the basic formulas of ionic conduction as discussed in section 2.2. Introducing a membrane to the system results in a barrier for ionic conduction, hence an extra resistance. Therefore an increase in resistance is expected to be measured in all cases upon introduction of the membrane. Proton hopping should not play a role in the total resistance of the system when salt concentrations are significantly higher than that of the protons and hydroxyl ions, because conduction is dominated by ion conductivity.

It is expected that the size and charge difference of the ions plays a role in the observed resistance of the system which deviates from the theoretically trend in conductivity that should be seen when looking at a membraneless system. Multivalent ions are expected to be attracted stronger by the Si-OH groups than single charged ions. Due to this stronger interaction transport is expected to be slower resulting in a larger increase in the systems resistance. Large ions are not excluded from transport as the pore size will not be small enough for this to happen, therefore no significant dependence is expected with respect to ion size. When the electrode surface and distance remains fixed the measured electrical resistance of the system should provide an indication of the impact due to the use of different electrolytes.

3. Experimental aspects

The first experiments were carried out using tapered shaped serpentine channels on a chip with electrodes placed in direct contact with the liquid. However, due to misalignment of the electrodes and fractures in the chip, it was not possible to measure accurately and reliably on this chips or to reproduce measurements. Therefore no results of the serpentine chips are evaluated and it was decided to change to more simple designed chips.

3.1. Fluidic set-up

All experiments in this report were carried out with in-house made X-shaped chips. These chips have a porous silicon membrane located at the middle of the X. A schematic representation of the X-shaped chip is shown in Figure 2. The chip was placed into a chip-holder as shown in Figure 3. The main pores formed in porous silicon have a branched network of smaller secondary pores, which interconnect the main pores. The main pores have a diameter in the range between 4 nm and 6 nm [9].

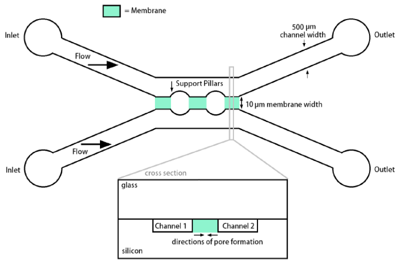

Figure 2 Schematic representation of X-shaped chip with horizontal oriented pores. The channels are etched into the silicon substrate with deep reactive ion etching. The channels are 500 µm in width. The porous silicon is 10 µm thick and high and 1 mm long. Top view and cross section, image is not on scale. [4]

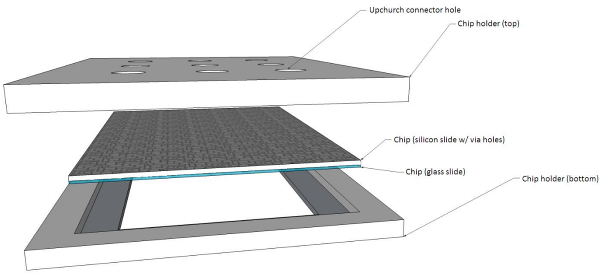

Figure 3 Chip in chip-holder [7]

Two BD (Becton, Dickinson and Company) plastic 3 mL syringes were filled with the electrolyte solution and placed into a Harvard syringe pump. The pump was adjusted to the syringe and the target volume (0.5 mL) and infuse rate (15 µL/min) were adjusted. The syringes were connected to the chip by fluid-connectors and capillaries (inlet). The outlet was connected with fluid-connectors and capillaries and collected in two small bottles. The capillaries did not touch the collected liquid in the bottles, which is important in order to prevent the ions from back diffusion and influencing the measurements.

3.2. Solutions

The experiments were carried out with different salt solutions; potassium chloride (KCl), calcium chloride ($CaCl_2$), sodium chloride (NaCl) and sodium sulfate (Na_2SO_4). KCl, CaCl and NaCl were obtained from Sigma Aldrich, Na_2SO_4 was obtained from Merck.

The respective molar conductivities of these salts are: 1.5, 2.72, 1.26 and 2.6 ($\Omega^{-1}\,m^2\,mol^{-1}$) [5]. 10mM solutions were prepared in 50 mL flasks with deionized (DI) water. The actual concentrations, respective theoretical specific conductivity and resistance are given in Table 2.

Table 2 Concentration and specific conductivity of salts

Salts	**Actual concentration (mM)**	**Theoretical specific conductivity ($\Omega^{-1}\boldsymbol{m}^{-1}$)**	**Resistance (Ωm)**
KCl	10.2	15.3	0.0654
$CaCl_2$	9.96	27.1	0.0369
NaCl	10.0	12.6	0.0794
Na_2SO_4	10.0	26.3	0.0380

3.3. Electrical measurements

Electrical measurements were performed to investigate ion transport through the porous silicon membrane. A potentiostat (PalmSense, Palm Instruments) was connected to platinum electrodes (equal electrode surface) which were connected to the outlet capillaries (they did not fit tight). The capillaries used have a diameter of 200 µm. A representation of the set-up is shown in Figure 4. No changes were made to the electrode connection and the same chip one with membrane and one without membrane was used in all experiments. Hence the resistance resulting from the electrode distance is kept constant in all measurements. This allows for a comparison between the effects of the different electrolyte on the membrane as the chips are similar.

Before each salt measurement, the capillaries were cleaned with DI water. During the cleaning the current vs. potential was measured. The cleaning was stopped when all the salt was removed from the capillaries which was obtained when the current reaches the level of DI water as measured in the first measurements with only DI water (-0.4 nA at -0.2 V).

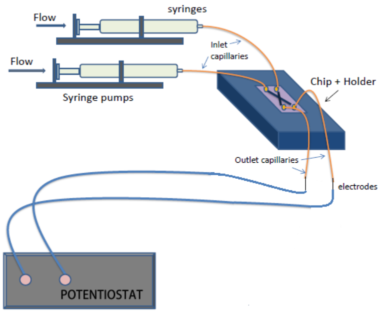

Figure 4 Set-up potentiometry measurements [4] (adapted)

The technique used for the measurements is Cyclic Voltammetry (CV). Current vs. potential was measured in the range of -0.2 till 0.2 V with a step size of 0.005 V and scan rate of 0.005 V/s. A graph was obtained with the potential (V) on the x axis and the Current (A) on the y axis. Resistance of the total system was obtained by determining the slope of the graph and using equation (5).

$$R = \frac{\Delta U}{\Delta I} \tag{5}$$

In this equation, R is the resistance (Ω), U is the potential (V) and I is the current (A).

4. Results

The raw data obtained from the CV measurements by the PSTrace program were presented in a graph of current vs. applied potential and accompanying dataset. In Figure 5 an example of the raw data graph is given. Each curve represents 1 CV cycle. Curve 1 is made when the DI water was just replaced with the salt solution and the DI water was still in the capillaries (-0.4 nA at -0.2 V). It is shown how the slope increases, when the salt solution enters the chip. The measurement was ended when the CV cycles stabilizes (this happened on average after 10 cycles). Since the electrodes were not fully covered or protected the signal was prone to disturbance by air circulation or surface reactions. These could have caused the deviating peaks in the current measurement.

Afterwards, the data obtained was transferred into Excel and the current vs potential was plotted again. For further calculations, we took the last CV cycle which was stable (or the one before if the last cycle contained deviating peaks). A linear trendline was drawn through the datapoints and with the slope and equation (5), the resistance was obtained. In Figure 6 an example of the processed data is shown.

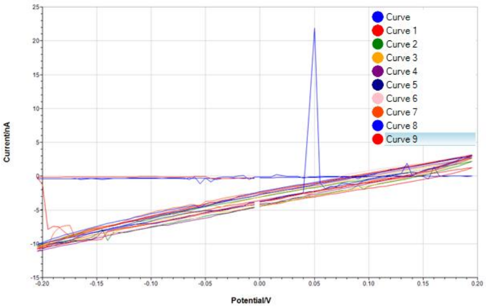

Figure 5 Example raw data, NaCl 10mM 15µL/min. Each curve represents 1 CV cycle.

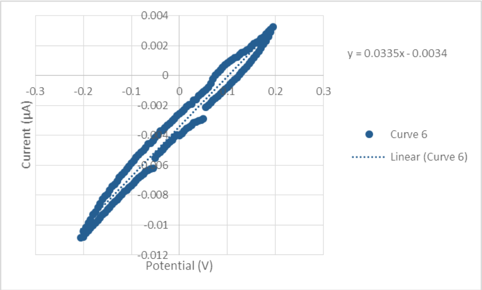

Figure 6 Example processed data

The obtained resistances are shown in Table 3. The resistance for the salts with a membrane is the average of two individual CV measurements. The resistance for DI water with and without membrane is the average of 6 individual CV measurements. The membrane resistance is obtained by subtracting the resistance without a membrane from the resistance with a membrane.

Table 3 Results voltammetry measurements

Resistance measurements (MΩ)			
	$R_{\text{without membrane}}$	$R_{\text{with membrane}}$	R_{membrane}
DI water	388	1,006	676
KCl	19.6	24.6	5.07
NaCl	14.4	30.3	15.8
$CaCl_2$	10.3	18.9	8.56
Na_2SO_4	18.9	26.4	7.57

Without a membrane the resistance increases from $CaCl_2$ < NaCl < Na_2SO_4 < KCl as is shown in **Error! Reference source not found.**, which does not agree completely with the theory of electrolyte resistance ($CaCl_2$< Na_2SO_4< KCl < NaCl).

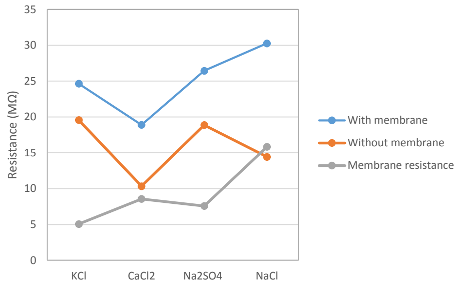

Figure 7 Resistance with membrane, without membrane and membrane resistance under influence of different salts

From the results it can be seen that the electrical resistance of the system with a membrane is higher than the resistance without a membrane, which is in accordance with the expectations set in section 2.3. It is also shown that the resistance with DI water is higher than the resistance with the different salts. This is explained by the presence of ions in the case of salts, resulting in a lower resistance and higher conductance.

With a membrane, the resistance increases from $CaCl_2$ < KCl < Na_2SO_4 < NaCl (**Error! Reference source not found.**), which is a different sequence than observed without a membrane.

The membrane resistance calculated by the difference in resistance with and without membrane, is clearly influenced by the salts, as the resistance is two orders higher in DI water than in the salt solutions. It is shown that the membrane resistance increases with decreasing cation size ($K^+ > Ca^{2+} > Na^+$), which is different than expected. The same is shown for anions, as the membrane resistance increases with decreasing anion size ($SO_4^{2-} > Cl^-$)

The influence of double charged cations is observed in the difference between NaCl and $CaCl_2$ measurements. Because they both have about the same size, the decrease in resistance can possibly be attributed to the presence of doubly charged ions.

5. Discussion

This project started with the use of the specially designed tapered chips. Although the design should help to improve the proton transfer and production of hydrogen, due to leakages and damages no good results could be obtained. First the production of these kind of chips should be improved, before actual measurements could be performed.

We expected that the resistance of the system without a membrane decreases with lower electrolyte resistance ($CaCl_2$< Na_2SO_4< KCl < NaCl) as given in section 3.2. However, the trend observed did not match this theory ($CaCl_2$< NaCl < Na_2SO_4< KCl). The results show big differences between similar measurements and error margins up to 10% are observed. Due to the possible error margins, which cannot be quantified because of to the lack of measurements, the observed trend may be rectified by providing error bars. Therefore more data is needed in order to draw a reliable conclusion on the influence of the different salt solutions within the membraneless system.

Addition of the porous silicon membrane resulted in a higher overall resistance, which was also in agreement with the expectations due to the extra barrier formed compared to the measurements without a barrier.

We expected that charge would have an influence on the resistance observed and the size of the ions would not. With a membrane, no clear trend was observed between the different salts. However, we did observe that the membrane resistance was both influenced by the charge and size of the ions. With regard to the ion size, we observed a trend were the resistance increases with decreasing cation size. Apparently, the size of the ion has an influence on the resistance. A higher charge seems to result in a lower resistance, which was opposite to what was expected.

Although more measurements are required, we are not convinced that multivalency of cation charge is less important than the cation size. When taking NaCl out of the results, the trends observed are much more in agreement to the one expected. Therefore we would suggest to repeat the measurements with NaCl, in order to find out if the measurements were not correct or that the behavior is just not as expected regarding the theory.

Since the trend in conductivity as a result of ionic contribution did not agree with the established theory and the results are rather doubtful several improvements to the setup are recommended. For one the electrodes were located at quite some distance from the membrane. Integrated electrodes would not only resolve this problem but also reduce the amount of disturbance that resulted from the use of the thin platinum electrodes which were partially exposed to the atmosphere. Although two similarly fabricated chips were used they were different and even minor discrepancies may have affected the overall resistance that was measured. The potentiostat was used at the limit of its range when measuring in the nA range. Therefore it is expected that the measurements were prone to some inaccuracies that resulted from the limitations of the equipment. Another potentiostat may have provided different results, however due to time limitations we were not able to test this.

When the setup is capable of operation at the required precision, additional measurements are to be performed. Every salt (concentration) should be measured at least five times in order to provide a reliable set of data. Although increasing the concentration of the salts would result in a more clear distinction to be made between the influences of the different salts, yet sedimentation and blockage resulting from the increased concentration should be kept in mind. Additional characterization of the chips resistance is also recommended by a current potential measurement in a dry chip. The resistance of the solution should also be checked in the bulk, using a fixed electrode distance and surface.

6. Conclusion

A conceptual method for measuring the resistance in an X-shaped microfluidic chip with a porous silicon membrane has successfully been proposed. However the electrode connections and positioning are to be improved before accurate measurements can be performed. It is shown that the resistance of the microfluidic system increases when a porous silicon membrane is used. The increase in resistance was most clearly observed when DI water is used as an electrolyte. Although the systems resistance also increased when using several salt solutions the difference was much lower. No clear trend was observed for the influence of different salts on the resistance with membrane. However, it was observed that both charge and size of the ions have influence on the membrane resistance. More measurements with an improved setup are needed to produce convincing results.

7. Literature

1. Bičáková, O. and P. Straka, *Production of hydrogen from renewable resources and its effectiveness.* International Journal of Hydrogen Energy, 2012. **37**(16): p. 11563-11578.
2. Prévot, M.S. and K. Sivula, *Photoelectrochemical Tandem Cells for Solar Water Splitting.* The Journal of Physical Chemistry C, 2013. **117**(35): p. 17879-17893.
3. Kajita, Y., et al., *Development of H2/O2 Generation Chip for Micro Fuel Cell Devices.* Proceedings of Micro Total Analysis System, 2011: p. 653-655.
4. Schildkamp, S.M., *Optimization of proton transport in solar water splitting reactors*, in *Mesoscale Chemical Systems Group*2014, University of Twente: Enschede.
5. Koper, M., *Course Notes: Electrochemistry and bioelectrochemistry*, 2015, University of Leiden.
6. Chinen, H., et al., *Enhancement of Proton Mobility in Extended-Nanospace Channels.* Angewandte Chemie International Edition, 2012. **51**(15): p. 3573-3577.
7. Wisman, S., *Comparison of proton conducting materials for micro solar fuel generators: Nafion and Porous silicon*, in *Mesoscale Chemical Systems Group*2014, University of Twente: Enschede.
8. Crittenden, J.C., et al., *MWH's Water Treatment: Principles and Design*. 2012: Wiley.
9. Tiggelaar, R., et al., *Characterization of porous silicon integrated in liquid chromatography chips.* Lab on a Chip, 2009. **9**(3): p. 456-463.

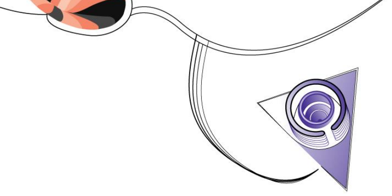

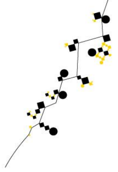

Cations transport in porous silicon

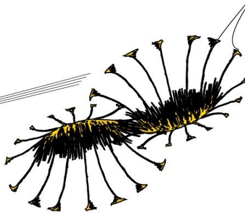

Zahra Heidarnia S1538357

Ratih Fauziah S1621432

Supervisors:

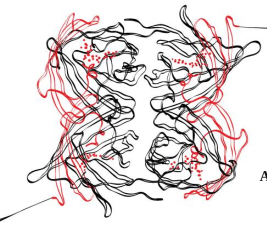

Dr. David Fernandez Rivas

Sebastiaan Wisman

Samuel Mok

AMM- Project Materials & Molecular S&T

June 2015

UNIVERSITY OF TWENTE.

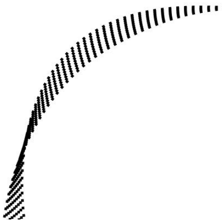

Contents

I. Introduction

Sustainable energy is an important discipline that has received considerable attention not just in the theory but in the practice. All over the world, there are numerous researches being conducted to find new ways which will make it possible to switch from conventional energy resources to sustainable ones. Considering solar energy as a source of permanent sustainable energy, is challenging due to its dilute, intermittent, and stochastic nature [1]. In order to be able to harvest the solar energy in a perfect way, we need to make it storable.

This study is part of a bigger project which is dedicated to "solar to fuel" devices. These devices use solar energy to split water and consequently produce hydrogen gas that can be stored as fuel. In this process, water is split into oxygen and protons at the anode and the protons are reduced to hydrogen at the cathode. The proper proton transport from anode to cathode is necessary for the whole reaction to be completed. Porous membranes are one of the possible solutions for cation transport. In this project, cation-transport properties of nano porous silicon membranes are characterized. The definition of some concepts used in this research are explained below.

i. Electrical Double Layer and ion transport in nanochannels

Solid surfaces with some functional groups, and a consequent fixed charge on them will maintain electrostatic interactions with free ions present in the fluid. As a result, the oppositely charged ions will create an electrical double layer on the solid surface (EDL).

Debye length is the characteristic length of the electrical double layer and is calculated by Equation 1 where ε is the permittivity of the solution, k_B is the Boltzmann constant, T is the absolute temperature, e the elementary charge, N_A is the Avogadro number, and I is the Ionic strength [2]. For calculation of I, equation 2 can be used where c_i is the molar concentration of ion I and z_i is the charge number of that ion. According to Eq. (1) the Debye length related to the ionic strength of the electrolyte and decreases with increasing the concentration.

$$\frac{1}{\kappa} = \sqrt{\frac{\varepsilon k_B T}{2e^2 N_A I}} \tag{1}$$

$$I = \frac{1}{2}\sum c_i z_i^2 \tag{2}$$

Applying a voltage to nanocannels will cause an electrical current which has two components, surface current (which is due to the counter ion transport) and bulk current. The former is highly dependent on the pore material and plays an important role in ion selectivity of the nanochannel [3]. In our case, the charged surfaces are the inner walls of the porous silicon membrane which are negatively charged.

Conductance ($G = {}^{I}/_{V}$) of an electrolyte is related to the number of free charge carriers, here ions. In the bulk K is proportional to the salt concentration (ionic strength). In the nanochannels with charged surfaces, however, the charges brought by the surface lead to a supplementary contribution to the conductance [4].

According to the work of Marins et al. [5], conductance of a nanochannel is the sum of electrical double layer (EDL) and bulk conductance. At very low ionic concentrations in nanochannels, the electrical double layers overlap, counterions easily pass through, whereas coions are repelled. This means that the electrical double layer thickness is lower than the pore diameter (h). In this situation, conductance of the electrolyte reaches a saturation value and remains constant. At higher concentrations, however, conductance increases with the concentration. This effect is shown in Figure 1.

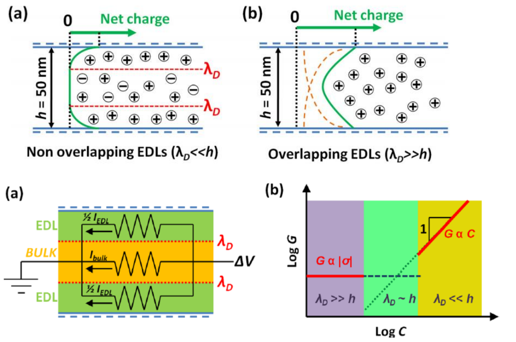

Figure 1 In the upper part a nanochannel with negatively charged isurface is shown. When the double layer thickness is higher than the pore diameter, the channel acts selectively and transforms counter ions only. Lowe part shows (a) the equivalent electric circuit model used to describe G which is the sum of two components: EDLs conductance and bulk conductance. (b) Nano channel ionic conductance vs. concentration. For EDL<<h G is constant and for EDL>>h, G increases linearly with concentratin [4].

II. Materials and methods

The goal of this experiment was to study the influence of the electrolyte concentration and electrolyte type on the cation conductivity of the silicon membrane. For this purpose, silicon microreactors with an implemented porous silicon membrane were used and the membrane resistance was measured for two types of different electrolyte, each with three different concentrations.

i. Preparation of the solution

Potassium Chloride (KCl) and Calcium Chloride ($CaCl_2$) electrolytes were prepared with three different concentration 1mM, 2.5 mM, and 5 mM. For each of the electrolytes, a 5 mM stock solution was made by dissolving the corresponding salt in Milli-Q water. The stock solution of each salt was then diluted with Milli-Q water to make 2.5 mM and 1 mM solutions.

ii. Electrical resistance measurement

In order to measure the effect of different electrolytes on membrane resistance, three different configurations were used for connecting the wires to the electrodes on the chip. A silicon chip with an in-built porous silicon membrane served as the selective proton/cation transport media was used for the measurements. The electrodes on the chip are platinum, since it is the best catalyst for producing hydrogen through water electrolysis and inert to almost all of chemical reactions and conducts electricity very well.

The chip was placed in the chip holder, fused silica capillaries (OD 360 μm/ID 100 μm) were connected to the chip through the chip holder and with the help of plastic rubber bands and ferrules. The two inlets of the chip were connected via the capillaries to the syringes (3 mL Beston D plastic) which were driven by a Harvard pump (Harvard Apparatus PHD2000). The syringes were filled with the solutions, the flow rate was assigned to 5 µl/min and then the pumping was started. A potential was applied to the system and the corresponding current was measured in a linear sweep mode. The potential range was set from -0.1 V to 0.1 V.

Before each measurement, in order to remove the remaining electrolyte in the chip and capillaries from the previous measurements, the capillaries were flushed with the next solution. The measurements were done in a two-electrode configuration in which the reference electrode of the potentiostat was short-circuited with the counter-electrode of the chip.

In order to connect the potentiostat to the electrodes three different methods were uses. First ferrules were used to connect the wires to the platinum electrode on the membrane. With this setup, since the wires were not connected properly to the electrodes, high amount of fluctuation were observed in the measured current. In order to get stable current data the connection between the wires and the platinum electrode was modified. In the second configuration, the electrode hole was filled with the corresponding electrolyte solution during the measurement. In the third method silver-epoxy, which is a conducting glue, was applied on the back side of the chip and leaved for 24 hours to be dried. The wires were again connected to the electrodes with ferrules.

In order to check if our data is reproducible we repeated this experiment on the next days. We disassembled and reassembled the system, flushed the system and started all the measurements again. All measurement conditions were the same as the previous one. This was only done for KCl, due to the limited time of the project.

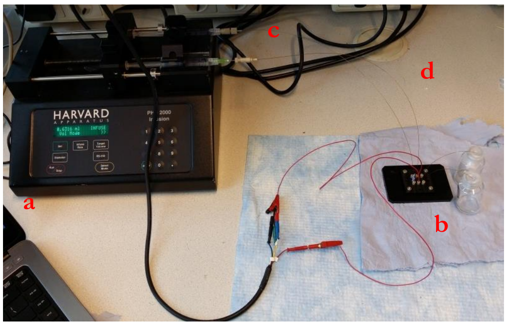

Figure 2 The measurement set up. The Harvard pump (a) is connected to the chip through the chip holder (b). Electrolyte in the syringes (c) is pumped to the chip via fused silica capillaries (d). The outlet flow of the chip is collected in plastic bottles.

III. Results and discussion

i. Ionic strength and Debye length effect

The theoretically calculated results for Debye length of each electrolyte at each concentration are shown in Table 1.

Table 1. Theoretical Debye Length for each electrolyte

Concentration (mM)	1/κ (nm)	
	KCl	$CaCl_2$
1	9.727	5.597
2.5	6.151	3.857
5	4.332	2.744

The obtained $I-V$ curves for three different concentrations of KCl and $CaCl_2$ electrolytes are shown in figures 3 and 4. (The reported data are measured with the silver-epoxy configuration. The data we obtained with the other configurations were not reproducible).

The slope of the $I-V$ curve gives the conductance ($G = {}^{I}/_{V}$) of the membrane which is the reciprocal of the membrane resistance. The experimental data in figures 3 and 4 illustrate the dependence of the conductance of the membrane (G) on the ionic strength of the solution. And it is obvious from the graph that for higher concentrations the resistance is higher. This can be explained by the double layer formation of the solution. The Debye length of both solutions decreases with increasing the concentration and this could explain the trend observed for the conductance versus concentration. When the radius of the channel is shorter than the Debye length, then the concentration of cations is much larger than that of anions everywhere within the channel. Larger differences between the Debye length of the channel and the channel radius, will result in higher selectivity of the channel and higher number of charge carriers.

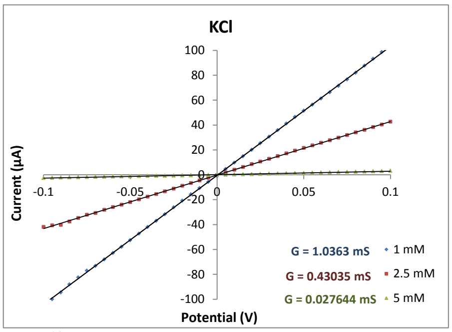

Figure 3 The obtained current versus the applied potential for the system with KCl electrolyte. The conductance of the membrane (G) decreases with the concentration.

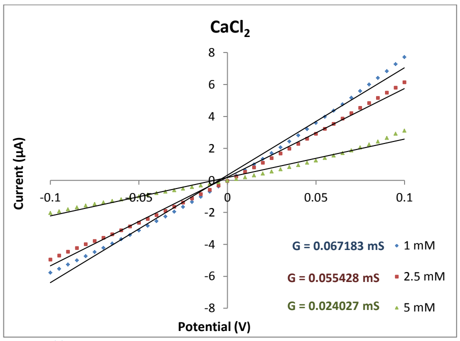

Figure 4 The obtained current versus the applied potential for the system with $CaCl_2$ electrolyte. The conductance of the membrane (G) decreases with the concentration.

The solutions with higher concentrations show lower conductance (thus higher resistance). This is in contrast with the literature [3], however they have used electrolytes that are in the saturated concentration. Our solution concentrations are less than saturated concentration, so this might be a reason for the inconsistency of our result with the literature. In the concentration range of our experiment (1 mM to 5 mM), the dominant conductance is the G_{EDL}. Hence, according to literature, we are in the plateau region and we should observe an approximately constant conductance [6].

The results for checking the reproducibility of the experiment are shown in Figure 5. The obtained resistance for each concentration is not the same with previous measurements. However, the increasing trend of the resistance from the low concentration to the higher ones is still the same. According to the curve, for every KCl concentration, the membrane resistances obtained in this measurement are higher than the first measurement. This could be due to salt residues from previous measurements on the membrane pores or capillary system. The salt blockage can happen because of inappropriate flushing process and salt mixing between KCl and $CaCl_2$. In order to check if the channels are blocked or not, they should be checked thoroughly under the microscope.

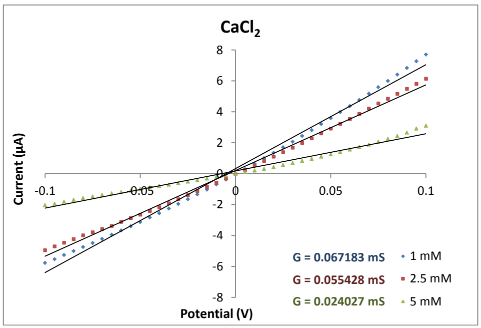

Figure 5 The result from KCl data reproducibility test. The decreasing trend of the membrane conductance with the concentration is the same, and the obtained conductance for each concentration is different from previous measurements.

In all the above graphs we see that in zero potential there is no current, and this is due to the same concentration of electrolyte in both syringes.

ii. Electrolyte Type Effect

In figure 6 to 8, the $I - V$ curves obtained for each concentration of the electrolyte are compared for KCl and $CaCl_2$ electrolyte. (red:$CaCl_2$, blue: KCl). the resistance value (1/G) between 1 mM and 2.5 mM of each solution, $CaCl_2$ always gives the higher resistance value, thus we can conclude that for the concentration we used, KCl has better conductance than $CaCl_2$.

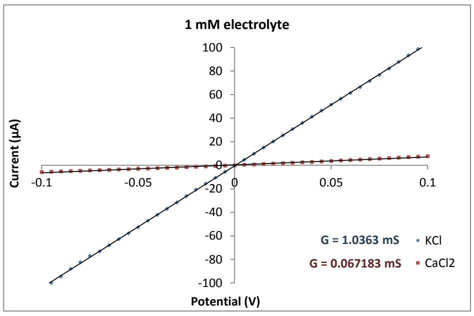

Figure 6 The effect of electrolyte type on the membrane conductance. G is obtained from the slope of the I-V curves. At same concentration, conductance of potassium chloride is higher than that of calcium chloride.

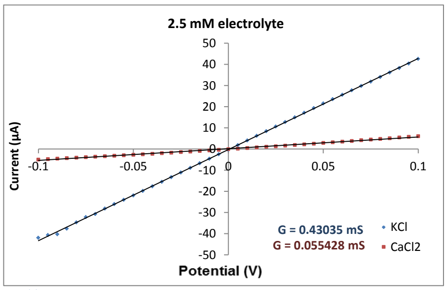

Figure 7 The effect of electrolyte type on the membrane conductance. G is obtained from the slope of the I-V curves. At same concentration, conductance of potassium chloride is higher than that of calcium chloride.

The difference between the membrane resistance for KCl and $CaCl_2$ can be explained by the ionic charge differences between K^+ and Ca^{2+}. According to Table 1 the Debye length of $CaCl_2$ for each concentration is lower than that of KCl solution with the same concentration. Debye length is a function of ionic strength, and ionic strength is dependent on the ion charge. The calcium ion has higher oxidation state leading to higher ionic strength and lower Debye length. When Debye length is higher than the pore's diameter, the membrane's conductance will be higher. For KCl solution 1mM and 2.5 mM concentrations, Debye length is higher than the pore's diameter of the silicon membrane (d = 6 nm), leading to higher conductance than $CaCl_2$.

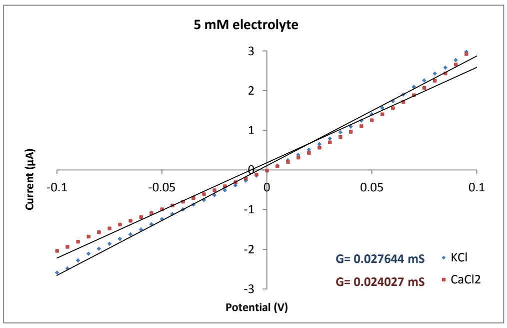

Figure 8 The effect of electrolyte type on the membrane conductance. G is obtained from the slope of the I-V curves. At same concentration, conductance of potassium chloride is higher than that of calcium chloride.

IV. Conclusion

In this experiment we analyzed the effect of ionic strength of the electrolyte on the proton conductivity of the porous silicon membranes embedded in the silicon chips for use in solar-2-fuel applications. We observed that the conductance of the membrane for a specific electrolyte increases with decreasing the concentration. Additionally, when comparing KCl and $CaCl_2$ we observed that conductance of the membrane is higher for KCl at every concentration which could be due to the higher Debye length of the KCl solution. The concentrations we used are in the plateau region of the conductance-concentration curve (< 1mM), and what we expected was a roughly constant conductance at different concentrations. However, for a more precise conclusion there should be more experiments done with more than three different concentrations in different orders of magnitude, to see the effect of the number of charge carriers on the membrane conductance.

As a suggestion for future work, first, the reproducibility of the obtained results should be investigated more in depth and the work can be continued with concentrations in the µm to mM range. As a new experiment, the effect of time on the membrane conductance could also be studied.

References

[1] Modestino, Miguel A., Camilo A. Diaz-Botia, Sophia Haussener, Rafael Gomez-Sjoberg, Joel W. Ager, and Rachel A. Segalman. "Integrated microfluidic test-bed for energy conversion devices." Physical Chemistry Chemical Physics 15, no. 19 (2013): 7050-7054.

[2] Tagliazucchi, Mario, and Igal Szleifer. "Transport mechanisms in nanopores and nanochannels: can we mimic nature?." Materials Today 18, no. 3 (2015): 131-142.

[3] Fuliński, A., I. Kosińska, and Z. Siwy. "Transport properties of nanopores in electrolyte solutions: the diffusional model and surface currents." New Journal of Physics 7, no. 1 (2005): 132.

[4] Bocquet, Lydéric, and Elisabeth Charlaix. "Nanofluidics, from bulk to interfaces." Chemical Society Reviews 39, no. 3 (2010): 1073-1095.

[5] Martins, D. C., V. Chu, and J. P. Conde. "The effect of the surface functionalization and the electrolyte concentration on the electrical conductance of silica nanochannels." Biomicrofluidics 7, no. 3 (2013): 034111.

[6] Yossifon, Gilad, Peter Mushenheim, Yu-Chen Chang, and Hsueh-Chia Chang. "Nonlinear current-voltage characteristics of nanochannels." Physical Review E 79, no. 4 (2009): 046305.